PRMT1-Mediated Metabolic Reprogramming Promotes Leukemogenesis

Hairui Su[1], Yong Sun[2,14], Han Guo[3], Chiao-Wang Sun[1], Qiuying, Chen[12], Szumam Liu[11], Anlun Li[11], Min Gao[4], Rui Zhao[1], Glen Raffel[5], Jian Jin[6], Cheng-Qui Qu[7], Michael Yu[13], Christopher A. Klug[8], George Y. Zheng[9], Scott Ballinger[2], Matthew Kutny[10], X. Long Zheng[11], Zechen Chong[4], Chamara Senevirathne[3], Steve Gross[12], Yabing Chen[2, 14]*, Minkui Luo[3,12]* and Xinyang Zhao[1,11]*

[1] Department of Biochemistry and Molecular Genetics, [2] Department of Pathology, [4] Department of Genetics, [8] Department of Microbiology, [10] Department of Pediatrics, The University of Alabama at Birmingham, School of Medicine, Birmingham AL 35294

[3]Tri-Institutional PhD Program of Chemical Biology; Chemical Biology Program, Memorial Sloan Kettering Cancer Center, New York, NY 10065

[5] Department of Medicine, University of Massachusetts, Cambridge, MA 02139

[6] Center for Therapeutics Discovery, Mountain Sinai Hospital, New York, NY USA

[7]Department of Pediatrics, Aflac Cancer and Blood Disorders Center, Children's Healthcare of Atlanta, School of Medicine, Emory University, Atlanta, GA 30322

[9] Department of Pharmaceutical and Biomedical Sciences, College of Pharmacy University of Georgia, Athens, GA 30602

[11]Department of Pathology & Laboratory Medicine, University of Kansas Medical Center, 3901 Rainbow Boulevard, Kansas City, KS 66160

[12]Program of Pharmacology, Weill Cornell Medical College of Cornell University, New York, NY 10021,

[13] Department of Biological Sciences, SUNY at Buffalo, Buffalo, NY

[14] Department of Pathology and Laboratory Medicine, Oregon Health and Science University; and Research Department, Portland Veterans Affairs Medical Center, Portland OR

* Corresponding coauthors

Abstract:

Copious expression of protein arginine methyltransferase 1 (PRMT1) is associated with poor survival in many types of cancers, including acute myeloid leukemia. We observed that a specific acute megakaryocytic leukemia (AMKL) cell line (6133) derived from RBM15-MKL1 knock-in mice exhibited heterogeneity in Prmt1 expression levels. Interestingly, only a subpopulation of 6133 cells expressing high levels of Prmt1 caused leukemia when transplanted into congenic mice. The PRMT1 inhibitor, MS023, effectively cured this PRMT1-driven leukemia. Seahorse analysis revealed that PRMT1 increased the extracellular acidification rate (ECAR) and decreased the oxygen consumption rate (OCR). Consistently, PRMT1 accelerated glucose consumption and led to the accumulation of lactic acid in the leukemia cells. The metabolomic analysis supported that PRMT1 stimulated the intracellular accumulation of lipids, which was further validated by FACS analysis with BODIPY 493/503. In line with fatty acid accumulation, PRMT1 downregulated the protein level of CPT1A, which is involved in the rate-limiting step of fatty acid oxidation. Furthermore, administering the glucose analogue 2-deoxy-glucose (2-DG) delayed AMKL progression and promoted cell differentiation. Ectopic expression of Cpt1a rescued the proliferation of 6133 cells ectopically expressing PRMT1 in the glucose-minus medium. In conclusion, PRMT1 upregulates glycolysis and downregulates fatty acid oxidation to enhance the proliferation capability of AMKL cells.

41 **Introduction:**

42 Normal hematopoietic stem/progenitor cell transformation to acute myelogenous leukemia (AML) cells
43 requires metabolic reprogramming (Kreitz et al., 2019). AML cells rely heavily on glucose for unchecked
44 proliferation. Using ^{18}F-Fluoro-deoxy-Glucose (^{18}FDG) as a marker, Cunningham et al. detected high
45 glucose uptake in the bone marrow of AML patients, and pyruvate and 2-hydroxy-glutarate concentrations
46 negatively correlate with patient survival rates (Chen et al., 2014). Dysregulated metabolic enzyme and
47 mitochondrial activities have been reported to be the causes of chemoresistance to AML (Jones et al.,
48 2019; Lagadinou et al., 2013) as well as solid tumors (Faubert et al., 2020). Metabolites such as acetyl-
49 CoA, α-ketoglutarate, vitamin C (aka ascorbic acid), and *S*-adenosyl-L-methionine (SAM) are cofactors for
50 histone and DNA modifications. Thus, metabolic reprogramming transforms the epigenetic landscape in
51 leukemia cells. Mutations in isocitrate dehydrogenases, IDH1/2, produce 2-hydroxyl-glutarate (2-HG)
52 instead of α-ketoglutarate. 2-HG inhibits demethylases that erase methylation marks on histones and DNA
53 and hydroxylases such as FIH (factor inhibiting HIF) in leukemia and glioblastoma (L et al., 2017).
54 However, mutations of metabolic enzymes in cancer are relatively rare. Usually, metabolic reprogramming
55 is achieved mainly by expressing oncogenic transcription factors such as p53 mutants, HIF1, and FOXOs
56 (Choi et al., 2012; Humpton et al., 2018; Laplante and Sabatini, 2013; Schwartzenberg-Bar-Yoseph et al.,
57 2004). Dysregulation of signaling pathways, such as KRAS mutations (Faubert et al., 2020; Ferrer et al.,
58 2014) and upregulation of the mTOR pathway during leukemogenesis (Kalaitzidis et al., 2012) , also alter
59 metabolic pathways in tumorigenesis. Nevertheless, how epigenetic regulators involved in leukemogenesis
60 regulate metabolic reprogramming still needs more research.

61 The protein arginine methyltransferase (PRMT) family has nine members, with PRMT1 responsible for
62 most of the enzymatic activity in mammalian cells. PRMT1 is an epigenetic regulator via methylation of
63 histone H4 and transcription factor RUNX1 (Wang et al., 2001; Zhao et al., 2008). The oncogenic roles of
64 PRMT1 have been demonstrated in many types of solid cancers (Avasarala et al., 2015; Baldwin et al.,
65 2012; Cho et al., 2012a; Cho et al., 2012b; Guendel et al., 2010; Karkhanis et al., 2011; Le Romancer et
66 al., 2008; Mitchell et al., 2009; Yang and Bedford, 2013; Yoshimatsu et al., 2011). The importance of
67 PRMT1 in leukemia has been shown in FLT3-ITD, AML1-ETO, and MLL-EEN-associated acute myeloid
68 leukemia and lymphoid leukemia (Cheung et al., 2007; He et al., 2019; Lin et al., 1996; Shia et al., 2012;
69 Zou et al., 2012). Targeting PRMT1 is effective in treating leukemia with splicing factor mutations (Fong et
70 al., 2019). PRMT1 expression levels are low in quiescent hematopoietic stem cells but are elevated in
71 stressed HSCs. Furthermore, the upregulation of PRMT1 enhances glycolysis through the methylation of
72 PFKFB3 (Watanuki et al., 2024). Yet, how PRMT1 is involved in cancer metabolic reprogramming has not
73 been explored, albeit the known role of PRMT1 in metabolic regulation in model organisms.

74 Phosphorylation of Hmt1 (PRMT1 ortholog in yeast) controls cell cycle progression in response to nutrition
75 signals (Butcher et al., 2006; Messier et al., 2013). PRMT1 in *Caenorhabditis elegans and Trypanosoma* is
76 responsible for methylation of proteins inside mitochondria, although PRMT1 is not inside mitochondria,
77 while PRMT1-null worms have dysfunctional mitochondria .(Fisk and Read, 2011; Sha et al., 2016). In
78 Trypanosomes, PRMT1 promotes glycolysis and is required for virulent infection (Kafkova et al., 2018).
79 When quiescent yeast re-entered fresh glucose-rich medium, Hmt1 the yeast PRMT1 homolog is among
80 nearly 240 genes that were induced (by ≥5-fold) in the presence of fermentable sugars like glucose,
81 suggesting its crucial role in supporting cells under rapid growth and fermentation conditions (Brejning et
82 al., 2003-03-11). When transitioning from glucose to non-fermentable carbon sources such as glycerol,
83 Hmt1 is downregulated, implying that is likely repressed to facilitate this vital adaptation (Roberts and
84 Hudson, 2006).

85 Acute megakaryoblastic leukemia (AMKL) is a subtype of AML with leukemia cells stuck at the
86 differentiation stage of immature megakaryocytes. It is a rare leukemia often associated with Down
87 syndrome. In cases not related to Down syndrome, AMKL is caused by chromosomal translocations.
88 Although AMKL can occur in adults, it occurs more commonly in children (Athale et al., 2001).
89 Chromosomal translocation t(1;22) that generates the RBM15-MKL1 fusion protein was discovered in
90 childhood AMKL (Ma et al., 2001; Mercher et al., 2001). RBM15-MKL1 is a fatal disease without available
91 targeted therapy.

92 Copious expression of PRMT1 is a poor prognostic marker for AML (Zhang et al., 2015; Zhu et al., 2019).
93 Furthermore, PRMT1 is expressed at an even higher level in AMKL than in other types of AML (Zhang et
94 al., 2015). Constitutive expression of PRMT1 blocks terminal MK differentiation (Zhang et al., 2015), while
95 inhibition of PRMT1 activity promotes terminal MK differentiation (Su et al., 2021). Thus, we hypothesize
96 that inhibiting PRMT1 activity could be a pro-differentiation therapy for AMKL. A leukemia cell line called
97 6133 is derived from Rbm15-MKL1 knock-in mice. When transplanted, 6133 cells can cause AMKL with
98 low penetrance (Mercher et al., 2009). Using this leukemia mouse model, we report here that the elevated
99 level of PRMT1 maintains the leukemic cells via upregulation of glycolysis and that leukemia cells with high
100 PRMT1 expression are vulnerable to the inhibition of fatty acid metabolic pathways.

101 **Results:**

102 **PRMT1 promotes the progression of RBM15-MKL1-initiated leukemia**
103 The 6133 cells can be transplanted into recipient mice to induce low penetrant leukemia with symptoms
104 closely recapitulating human AMKL (Mercher et al., 2009). To find additional factors needed to transform

105 6133 cells fully, we have reported a fluorescent probe (E84) that can be used to sort live cells according to
106 PRMT1 protein concentrations (Su et al., 2018) (Supplemental Figure 1). We sorted 6133 cells into two
107 populations for bone marrow transplantation (BMT) according to E84 staining intensities (Figure 1A). All
108 mice that received 6133 cells expressing higher levels of PRMT1 (6133/PRMT1 cells) developed leukemia
109 and died rapidly, while 6133 cells expressing lower levels of PRMT1 did not develop leukemia (Figure 1B).
110 Consistently, a higher percentage of leukemia cells were detected in bone marrow and peripheral blood in
111 recipient mice transplanted with E84-high (i.e., density staining of E84) 6133 cells according to FACS
112 analysis (Figure 1C).

113 Given that E84-high cells can initiate leukemia, we introduced PRMT1 into 6133 cells (aka 6133/PRMT1
114 cells) using a lentivirus vector. Overexpression of PRMT1 rendered 6133/PRMT1 cells to increase in a
115 cytokine-independent fashion in cell culture (Figure 1 D), and recipient mice transplanted with 6133/PRMT1
116 cells developed leukemia and died within 25 days (Figure 1 E&F). Although PRMT1-mediated methylation
117 triggers the degradation of RBM15, PRMT1 overexpression does not affect the stability of the RBM15-
118 MKL1 fusion (Supplemental Figure 2 A&B). The leukemic mice displayed splenomegaly. Intriguingly, the
119 leukemia mice were paralyzed with observable spinal bleeding during dissection, although the bone density
120 was still normal (data not shown). In a xenograft model with human RBM15-MKL1 leukemia cells, leukemia
121 also caused spinal bleeding (Thiollier et al., 2012). Collectively, PRMT1 is essential for the initiation of overt
122 AMKL expressing the RBM15-MKL1 fusion protein, and leukemia initiated by 6133/PRMT1 cells in mice
123 resembles several characteristics of human AMKL.

124 **MS023, a PRMT1 inhibitor, cures mice with Rbm15-MKL1-initiated leukemia**

125 MS023 was reported to be a potent inhibitor of Type-I PRMTs including PRMT1 (Eram et al., 2016; Su et
126 al., 2021). Furthermore, MS023 has been tested safe on mice at 80 mg/kg of body weight (He et al., 2019;
127 Su et al., 2021). The 6133/PRMT1 cells were intravenously injected into sub-lethally irradiated recipient
128 mice. A week after bone marrow transplantation (BMT), we injected MS023 intraperitoneally every other
129 day for a month. Notably, while the untreated group of mice exhibited rapid illness and developed moribund
130 symptoms, such as severe weight loss and rear limb paralysis, within 30 days, the majority of mice treated
131 with MS023 remained healthy and symptom-free. Treatment with MS023 significantly alleviated the
132 leukemia burden, as shown by FACS analysis of the percentages of leukemia cells in bone marrow and
133 peripheral blood (Figure 2D). We also validated that the bone marrow cells from MS023-treated mice had
134 reduced global levels of arginine methylation (Supplemental Figure 1C). Leukemia-associated
135 splenomegaly was also alleviated in MS023-treated mice (Figure 2D). Kaplan-Meier curves showed that
136 the MS023-treated group was effectively cured after 120 days (Figure 2C), with only residual leukemia cells

137 detected in bone marrow and peripheral blood (Figure 2 D&E). Expression of c-MPLW515L mutant in 6133
138 cells can render the 6133 cells fully penetrant for leukemia (Mercher et al., 2009), and in vitro treatment
139 with MS023 reduced their proliferation (Figure 2F). Subsequently, we transplanted 6133/cMPLW515L cells
140 into congenic mice. Figures 2 G-I illustrate that MS023 also cures leukemia, suggesting that PRMT1 could
141 be a valid target for leukemia or myeloid proliferative diseases driven by c-MPLW515L. Collectively, these
142 data demonstrate that PRMT1 is critical for sustaining Rbm15-MKL1-initiated leukemia in mice, and
143 pharmacological targeting of PRMT1 represents an effective strategy for treating leukemia.

144 **PRMT1 promotes glycolysis in leukemia cells**

145 Given that the role of PRMT1 in metabolic regulation has been well-documented, we then investigated
146 whether PRMT1 is involved in transforming 6133 cells through metabolic reprogramming. To assess this,
147 we conducted Seahorse assays to measure the changes in ECAR (extracellular acidification rate) in
148 6133/PRMT1 cells compared to the parental 6133 cells. The ECAR curve of 6133/PRMT1 cells was
149 elevated compared to that of 6133 cells (Figure 3A). Interestingly, the addition of FCCP, which uncouples
150 oxidative phosphorylation from the TCA cycle, did not increase acidification levels. Similarly, antimycin did
151 not cause a significant drop in acid concentration. Remarkably, we treated 6133 cells with MS023 overnight
152 prior to Seahorse assays and observed a reduction in ECAR levels (Figure 3B). These findings suggest
153 that PRMT1 is responsible for the observed increase in acidification. In this experiment, glycolysis
154 contributes the most to acidification in the 6133 leukemia cells, as the addition of mitochondrial respiratory
155 inhibitors only moderately reduces acidification levels according to the principles outlined (Divakaruni et al.,
156 2014). Lactate dehydrogenase A (LDHA), the final key enzyme in glycolysis that converts pyruvate to
157 lactate for NAD+ regeneration, was found to be influenced by PRMT1 overexpression. Specifically, PRMT1
158 overexpression stimulated the tyrosine phosphorylation of LDHA, thereby activating its enzymatic activity
159 (Fan et al., 2011) despite an overall decrease in LDHA levels (Figure 3C). Consistently, when we directly
160 measured the intracellular and extracellular lactate levels in 6133 and 6133/PRMT1 cells, we observed that
161 6133/PRMT1 cells not only released more lactate into the medium but also exhibited higher intracellular
162 lactate levels (Figure 3D). We concluded that PRMT1 promotes cellular glycolysis and lactate production,
163 which predominantly contributes to the observed increase in acidification.

164 **PRMT1 reduces oxygen consumption in mitochondria**

165 The Seahorse assays have demonstrated that the cellular OCR (oxygen consumption rate) was reduced in
166 6133/PRMT1 cells. Additionally, it was observed that these cells had a limited capacity for reserve
167 respiration, as the maximum respiration level was nearly identical to the basal OCAR level, regardless of
168 the expression levels of PRMT1 (Figure 4A). Conversely, when the 6133/PRMT1 cells were pre-treated

169 with MS023 overnight before the Seahorse assays, there was an increase in mitochondrial oxygen
170 consumption compared to the non-treated controls (Figure 4B). These findings further support the notion
171 that PRMT1 plays a role in mediating metabolic reprogramming by enhancing glycolysis and reducing
172 mitochondrial oxygen consumption.

173 We demonstrated that PRMT1 increases the number of mitochondria in MEG-01 cells, a human acute
174 megakaryocytic leukemia cell line, by confocal microscopy (Zhang et al., 2015). In this experiment, FACS
175 analysis with MitoTracker staining (Figure 4C) and real-time PCR analysis of mitochondrial DNA (Figure
176 4D) further validated that PRMT1 upregulated mitochondrial biogenesis in 6133 cells. H2DCFDA staining
177 showed that PRMT1 elevated global ROS levels in 6133 cells (Figure 4F). Interestingly, when we
178 performed Mito-Sox staining for ROS levels within mitochondria, we found reduced levels of ROS (Figure
179 4G). These data imply that most of the ROS detected by H2DCFA may be generated from the cytoplasm
180 rather than from mitochondria, which aligns with the Seahorse data indicating that oxidation consumption in
181 mitochondria is reduced (Figure 4A). Next, we conducted TMRE staining for mitochondrial membrane
182 potential. 6133/PRMT1 cells exhibited reduced staining, suggesting that PRMT1 decreases membrane
183 potential (Figure 4E). This result also cross-validated the Seahorse findings that PRMT1 reduced
184 mitochondrial oxygen consumption.

185 Since the cytoplasmic ROS level significantly increased with PRMT1 expression, we measured the ratios of
186 two redox pairs: glutathione and $NADP^+$. Interestingly, activation of PRMT1 raised the ratios of both
187 GSH/GSSG and $NADPH/NADP^+$. Given the crucial roles of GSH and NADPH in biomass synthesis, the
188 upregulation of PRMT1 may promote anabolism, consistent with PRMT1's role in supporting cell
189 proliferation.

190 **Metabolomic analysis of PRMT1-induced metabolic changes**

191 To further probe the complexity of PRMT1-mediated metabolic reprogramming, we established a new 6133
192 cell line that can conditionally express PRMT1 upon adding doxycycline to the medium. We compared the
193 metabolomic status of 6133 cells before and after 12 hours of PRMT1 induction. The cells were grown in
194 standard RPMI1640 medium with 10% fetal bovine serum, with high concentrations of glucose and
195 essential amino acids for 12-hour growth. We repeated the metabolomic analysis five times. Principle
196 component analysis (PCA) indicated that PRMT1 caused a significant shift in metabolite profiles (Figure
197 5A,B, see supplemental table 1). Notably, PRMT1 activation led to increased ATP production and the
198 accumulation of succinyl-CoA, alanine, serine, and short-chain fatty acids and depletion of SAM, aspartic
199 acid, nicotinamide, succinyl-homoserine, oxidized glutathione (which is consistent with the increased ratio

200 of GSH/GSSG shown in Figure 4H), and alpha-ketoglutarate (aka oxoglutaric acid) (Figure 5C). These
201 findings suggest that the beta-oxidation of fatty acids may be impaired, leading to the accumulation of fatty
202 acids such as docosadiencic acid, caproic acid and suberic acid, while the levels of palmitoyl-carnitine are
203 reduced. Furthermore, the reduced levels of alpha-ketoglutarate indicate potential alterations in the TCA
204 cycle and glutaminolysis. Overall, our data highlights the profound metabolic changes induced by PRMT1,
205 particularly in amino acid biosynthesis, one-carbon metabolism as shown in Figure 5D generated by the
206 metaboAnalyst software (Pang et al., 2024).

207 **PRMT1-transformed leukemia cells are highly dependent on glucose consumption.**

208 After determining that glycolysis was enhanced in PRMT1-overexpressing cells, we performed glucose
209 colorimetric assays to measure glucose concentrations in the cell culture medium when the 6133 and
210 6133/PRMT1 cells grew exponentially. A more significant reduction of glucose in 6133/PRMT1 cells was
211 observed compared to parental 6133 cells (Figure 6A), indicating that the elevated glucose consumption
212 via glycolysis is due to PRMT1 upregulation. Next, we cultured the cells in both glucose-containing and
213 glucose-depleted media. Cell viability assays showed that 6133/PRMT1 cells grew more slowly in a
214 glucose-free medium, while parental cells were less affected (Figure 6B). Accordingly, we used 2-deoxy-D-
215 glucose (2-DG), a glucose analog that competes with glucose in glycolysis. The proliferation of
216 6133/PRMT1 cells was notably inhibited by 2-DG, while the proliferation of 6133 cells was barely affected
217 (Figure 6C). These results are consistent with Seahorse analysis indicating that 6133/PRMT1 cells rely on
218 glycolysis for growth (Figure 3). Next, we tested whether blocking glucose could impede AMKL progression
219 in mice. Four days after the transplantation of the 6133/PRMT1 cells, we administered 2-DG to the mice at
220 a dosage of 0.5g/Kg body weight every other day for a month. 2-DG treatment significantly delayed
221 disease progression (Figure 6D). Splenomegaly was alleviated, and the burden of leukemia cells in the
222 bone marrow and peripheral blood was notably decreased in the 2-DG treated mice (Figure 6E&F). Taken
223 together, the in vitro and in vivo data suggest that PRMT1-mediated metabolic reprogramming renders
224 leukemia cells highly dependent on glucose.

225 **Targeting fatty acid metabolic pathways for leukemia therapy**

226 Rapidly growing cancer cells need de novo synthesis of fatty acids to meet the demand for building cell
227 membranes (Menendez and Lupu, 2007). De novo fatty acid synthesis uses acetyl-CoA generated from
228 fatty acid oxidation. Inhibition of fatty acid oxidation has been shown to kill leukemia cells (Samudio et al.,
229 2010). Carnitine-palmitoyl-transferase (CPT1A) catalyzes the rate-limiting step of fatty acid oxidation by
230 transporting fatty acids across the mitochondrial outer membrane. RBM15 binds to the 3' UTR of CPT1A
231 mRNA (Zhang et al., 2015). Furthermore, PRMT1 regulates the stability of the RBM15 protein. We

232 demonstrated that the expression of both isoforms of PRMT1 lowered the mRNA levels of CPT1A (Figure
233 7A). We then performed Western blotting and confirmed that the protein level of CPT1A was
234 correspondingly reduced in 6133 cell lines ectopically expressing PRMT1 isoforms (Figure 6B). The
235 downregulation of CPT1A leads to reduced consumption of long-chain fatty acids. We consistently
236 observed greater lipid accumulation in 6133/PRMT1 cells than in 6133 cells through FACS analysis with a
237 lipid-binding fluorescent dye i.e. BODIPY 493/503 (Figure 7C). Metabolomic analysis also indicated the
238 accumulation of fatty acids such as suberic acid and caproic acid, alongside a decrease in palmitoyl-
239 carnitine, which is a product of CPT1A (see supplemental table 1 for metabolomic data). We then treated
240 leukemia cells with etomoxir, which inhibits CPT1A enzymatic activity. The 6133/PRMT1 cells were more
241 sensitive to etomoxir than the 6133 cells (Fig 6D). Orlistat, a FASN inhibitor, also suppressed the
242 proliferation of 6133/PRMT1 cells more effectively than that of 6133 cells (Fig 6E). While CPT1A is
243 responsible for transporting long-chain fatty acids, short-chain fatty acids can be directly transported to
244 mitochondria. We added acetate, propionate, and butyrate in the form of triglycerides to a glucose-free
245 medium. Strikingly, all three forms of short-chain fatty acids supported the proliferation of 6133/PRMT1
246 cells better than the parental 6133 cells (Fig 6F). The data suggest that leukemia cells with elevated levels
247 of PRMT1 expression can utilize short-chain fatty acids to compensate for their need for glucose.
248 We then used a lentivirus to express CPT1A in 6133/PRMT1 cells ectopically. CPT1A wild type and mutant
249 (H473A) that does not have succinylation activity (Kurmi et al., 2018) dampens the proliferation rates of
250 6133/PRMT1 cells cultured under standard conditions. Intriguingly, the enzymatically inactive CPT1A
251 mutant (G710E) inhibits the proliferation of the 6133/PRMT1 cells, suggesting that the 6133 cells still rely
252 on fatty acid oxidation for de novo lipid synthesis necessary for proliferation (Figure 7G). Taken together,
253 we demonstrated that although PRMT1 downregulates fatty acid oxidation as an energy source, PRMT1
254 upregulates using short-chain fatty acids as an alternative energy source for mitochondria.

255 **Discussion:**

256 This report demonstrates that PRMT1 promotes glycolysis and reprograms mitochondrial metabolism to
257 support leukemia progression in mice with RBM15-MKL1-initiated leukemia. Notably, only leukemia cells
258 with elevated levels of PRMT1 can be transplanted to initiate leukemia (Figure 1). This indicates that
259 PRMT1 assists leukemia cells in adapting to the bone marrow niche necessary for leukemia initiation,
260 suggesting that leukemia stem cells likely express high levels of PRMT1. Moreover, since normal
261 hematopoietic stem cells express low levels of PRMT(Su et al., 2018), targeting this protein may help
262 protect normal hematopoietic stem cells from damage. Considering the crucial role of PRMT1 in acute
263 myeloid leukemia (AML) with various gene mutations—including RBM15-MKL1, FLT3-ITD, MLL-EEN, and

264 AML1-ETO fusions—as well as mutations in splicing factor(Fong et al., 2019), PRMT1-mediated metabolic
265 reprogramming may be significant for the previously mentioned AML.
266
267 The potential mechanism of PRMT1-mediated metabolic reprogramming can be learned from published
268 data. PRMT1 methylates phosphoglycerate kinase 1 (PGK1) at arginine 206, which enhances its
269 phosphorylation at serine 203 (Liu et al., 2024). Additionally, PRMT1 methylates phosphoglycerate
270 dehydrogenase (PHGDH) at arginine 236, activating the enzyme and stimulating the synthesis of serine
271 (Wang et al., 2023; Yamamoto et al., 2024). Furthermore, PRMT1-mediated methylation of glyceraldehyde
272 3-phosphate dehydrogenase (GAPDH) prevents its localization in the nucleus of LPS-activated
273 macrophages, protecting these macrophages from apoptosis (Cho et al., 2018). Overall, these findings
274 underscore PRMT1's significant role in boosting glycolytic activity and tumorigenesis through the targeted
275 methylation of glycolytic enzymes.
276
277 RBM15 plays a crucial role in regulating the homeostasis of hematopoietic stem cells and the differentiation
278 of megakaryocytes. Our previous paper in eLife demonstrated that RBM15 is methylated by PRMT1, and
279 this modification affects RBM15-mediated RNA splicing of key transcription factors, including RUNX1,
280 GATA1, TAL1, and TPOR (also known as c-mpl), which are essential for megakaryocyte development
281 (Zhang et al., 2015). Notably, we found that nearly 50% of RBM15 targets are metabolic enzymes, with
282 their mRNAs' 3' UTR regions bound by RBM15. Among these targets, CPT1A mRNA stands out as
283 particularly significant. Our metabolomic analysis indicated that overexpression of PRMT1 leads to an
284 accumulation of intracellular lipids (Figure 5C). Consistently, we also observed that PRMT1 downregulates
285 the CPT1A protein level (Figure 7A,B) and detected lipid accumulation (Figure 7C) using FACS analysis.
286 Our unpublished data further validate that PRMT1 downregulates CPT1A in platelets expressing high
287 levels of PRMT1.
288
289 Although PRMT1 reduces oxygen consumption and membrane potential (Figure 4), it does not fully inhibit
290 the tricarboxylic acid (TCA) cycle or the electron transport chain. Cells expressing PRMT1 (designated as
291 6133/PRMT1) continue to proliferate using galactose, which does not produce ATP via glycolysis in
292 glucose-deficient medium. Moreover, the 6133/PRMT1 cells can thrive on glycerol combined with
293 substrates such as acetate (in the form of triacetin), propionate (tripropionin), and butyrate (tributyrin),
294 indicating that mitochondria can still utilize short-chain fatty acids (Figure 7G). These are converted into
295 acetyl-CoA, propionyl-CoA, and butyryl-CoA, which can then enter the TCA cycle independently of
296 CPT1A. This adaptation allows 6133/PRMT1 cells to consume short-chain fatty acids and non-fermentable
297 carbon sources like glycerol and galactose in glucose-deficient medium when CPT1A is downregulated.

298

299 RBM15 also binds to several mRNAs that encode enzymes involved in glycolysis, such as LDHA and HK1.
300 Although we did not detect increased protein expression of HK1 and LDHA, we observed an increase in
301 the tyrosine phosphorylation of lactate dehydrogenase A (LDHA) by PRMT1. Phosphorylation is known to
302 activate LDHA, indicating that PRMT1 upregulation enhances glycolytic flux. The decreased NADP/NADPH
303 ratio and aspartate concentration suggest a metabolic shift favoring glycolysis in proliferating cells.
304

305 The accumulation of succinate and the corresponding decrease in aspartate and alpha-ketoglutarate
306 levels, as demonstrated by PRMT1 overexpression, is consistent with findings from earlier research
307 involving T cells that have undergone succinate dehydrogenase (SDH) knockout (Chen et al., 2022). This
308 alteration inhibits α–KG–dependent dioxygenases, including Jumonji-domain histone demethylases and
309 DNA demethylases (such as TET), vital for the demethylation of histones and DNA. As a result, this affects
310 chromatin accessibility and influences gene expression patterns. We propose that changes in SDH activity
311 may allow PRMT1 to modify the epigenetic landscapes of mammalian cells indirectly in response to
312 metabolic shifts. Given the succinate accumulation, we expect that the HIF1α complex will be stabilized,
313 leading to pseudohypoxia phenotypes in cells with elevated PRMT1 expression, akin to those seen in
314 patients with myelodysplastic syndromes (MDS) (Hayashi et al., 2018). Furthermore, our findings indicate
315 that PRMT1 expression is significantly increased in samples from MDS patients (Su et al., 2021).
316

317 PRMT1-mediated metabolic reprogramming indicates that mitochondria in PRMT1-overexpressing cancer
318 cells primarily function to produce biosynthetic precursors instead of generating oxidative ATP. Our findings
319 further support that PRMT1 overexpression promotes mitochondrial biogenesis, as previously reported and
320 validated here (Figure 4C and D). However, the increase in mitochondrial quantity did not correlate with
321 increased oxygen consumption. Instead, we observed lower mitochondrial ROS levels per cell, consistent
322 with reduced mitochondrial membrane potential and decreased oxygen consumption. Mitochondria play a
323 crucial role in cancer cell metabolism, functioning not only as powerhouses for ATP production but also as
324 central hubs for metabolic intermediates vital for biomass synthesis. While many cancer cells display a
325 glycolytic phenotype, known as the Warburg effect, mitochondria remain essential for sustaining cell
326 proliferation.
327

328 Intriguingly, although mitochondrial ROS levels were reduced, we detected an overall increase in
329 cytoplasmic ROS. Since lipid accumulation can stimulate ROS generation (Liu et al., 2015), we speculate
330 that intracellular lipid accumulation due to PRMT1 overexpression may drive the increased cytoplasmic
331 ROS levels we observed in Figure 4. The regulation of oxidative stress by PRMT1 appears to involve a

332 complex interplay between mitochondrial function, lipid metabolism, and glycolytic flux. In cancer cells with
333 high PRMT1 expression, mitochondria may function as biosynthetic factories, channeling metabolic
334 intermediates for nucleotide, amino acid, and lipid synthesis rather than oxidative phosphorylation.
335 Understanding the precise mechanisms by which PRMT1 regulates metabolic pathways and redox
336 homeostasis may open new therapeutic avenues for targeting metabolic vulnerabilities in cancer.
337
338 The main limitation of this study is that we used only one mouse leukemia cell line for the metabolic
339 investigation. In our unpublished data, we have examined the expression of CPT1A in megakaryocytes and
340 platelets derived from Pf4-cre PRMT1 transgenic mice. Additionally, we validated that PRMT1
341 downregulated CPT1A in the megakaryocyte lineages. Considering that RBM15 and PRMT1 are
342 expressed in mammalian cells across different species, we suggest that the PRMT1-mediated metabolic
343 programming is conserved.

344

345 **Acknowledgement:**

346 The project was partially supported by the Leukemia Research Foundation, NCI R21 CA202390, and the
347 Elsa Pardee Foundation. ML is supported by the NIH R35 grant GM131858. YC is supported by NIH grants
348 HL146103, HL158097, HL167201, and AG082839, as well as the United States Department of Veterans
349 Affairs research awards BX005800, BX004426, BX006321, and CX002706 (to Y.C.). We would like to
350 thank Dr. Taro Hito Hitosugi (Mayo Clinic) for the CPT1A cDNAs.

351 **Methods and Methods**

352 <u>Cell Culture and metabolite measurement</u>

353 6133 cells were cultured in RPMI1640 medium supplemented with 10% FBS100 U/mL penicillin and 100
354 μg/mL streptomycin. The addition or withdrawal of mSCF (10 ng/mL) in the culture was performed
355 accordingly. The L-Lactate Assay Kit (Cayman, Ann Arbor, Michigan) was used to measure the intracellular
356 and extracellular lactate levels of the cultured cells: approximately $1x10^7$ cells were cultured in 10 mL of
357 fresh medium for 24 hours; the cell pellet and medium were collected and processed separately as
358 instructed. The Glucose Colorimetric Assay Kit (Cayman, Ann Arbor, MI) was used to quantify the
359 remaining glucose in the culture medium: $1.25x10^5$ cells were cultured in fresh medium overnight; the
360 supernatant/medium was collected and processed as instructed. The fluorescent or colorimetric signals
361 from the assays mentioned above were measured using a microplate reader (Biotek, Winooski, VT). The

362 ratio of NADP/NADPH was assessed using a kit (Cat# MAK479, MilliporeSigma). A total of 6133 cells (0.1
363 million) grown in the exponential phase were harvested for the assay in a 96-well plate according to the
364 manufacturer's instructions. The ratio of glutathione GSH/GSSG was determined following the
365 manufacturer's instructions (Cat# MAK440, MilliporeSigma).

366 Viral Production and Cell Line Selection

367 For lentivirus production as described (Su et al., 2021), viral vectors were co-transfected with the envelope
368 vector pMD2.G and the packaging vector ps-PAX2 into 293T cells. Fresh or concentrated viruses were
369 then used to infect the target 6133 cell lines. Stable cell lines were selected using GFP-based flow
370 cytometry sorting with the BD FACSAria II system (BD, Franklin Lakes, NJ).

371

372 Murine Leukemia Model and Treatments

373 GFP-positive 6133 cells were intravenously transferred into 8- to 12-week-old sub-lethally irradiated (6 Gy)
374 C57BL/6 mice. Disease progression was closely monitored on a daily basis. Moribund mice were sacrificed
375 to further analyze GFP-positive donor leukemia cells in the peripheral blood, bone marrow, and spleen. For
376 PRMT1 inhibitor treatment, 80 mg/kg body weight of inhibitor solution (16 mg/mL) was intraperitoneally
377 injected into recipient mice every other day for one month, starting on the fourth day post-cell transfer. The
378 PRMT1 inhibitor was dissolved in saline with 20% Captisol, 20% PEG-400, and 5% NMP (v/v). For 2-DG
379 treatment, 0.25 g/kg body weight of 2-DG (saline solution) was intraperitoneally injected into recipient mice
380 every other day for one month, beginning on the fifth day post-cell transfer.

381

382 Flow Cytometry Analysis

383 FACS analysis was conducted using the BD LSRFortessa (BD, Franklin Lakes, NJ). MitoTracker DeepRed
384 FM and TMRE stains (Molecular Probes, Eugene, OR) were employed to evaluate cellular mitochondria.
385 H2DCFDA dye (Cat#D399 ThermoFisher) was used to quantify cytoplasmic ROS levels. BODIPY™
386 493/503 (4,4-Difluoro-1,3,5,7,8-Pentamethyl-4-Bora-3a,4a-Diaza-s-Indacene) (ThermoFisher) was added
387 at a final concentration of 1 μM and incubated with 6133 and 6133/PRMT1 cells during the
388 exponential phase for 15 minutes at 37°C in the dark. After incubation, the cells were washed with
389 PBS twice before being subjected to FACS analysis using the manufacturer-recommended
390 spectrum filters.

391 Dr. Zheng's laboratory at University of Georgia synthesized E84, storing a 5 mM stock solution of E84 in
392 dimethyl sulfoxide (DMSO) at -20°C. Exponentially growing cells were harvested and washed with ice-cold

393 phosphate-buffered saline (PBS). E84 was then incubated at a final concentration of 10 nM with 5×10^5
394 cells in 100 μL of PBS on ice for 30 minutes. Afterward, the cells underwent two additional washes with
395 PBS, and the labeled cells were immediately used for cell sorting and fluorescence-activated cell sorting
396 (FACS) analysis. The FACS parameters included a laser wavelength of 640 nm, along with a filter set of
397 650 LP + 670/14. Fluorescence measurements were collected using the allophycocyanin (APC) channel on
398 the BD LSRFortessa machine (BD, Franklin Lakes, NJ). The FACS data were analyzed with FlowJo
399 software, and cell sorting was performed on a BD Aria II sorter.

400 SDS-PAGE and Western Blotting

401 6133 cells were collected from culture and lysed in 1 mL of H-Lysis buffer (20 mM HEPES pH 7.9, 150 mM
402 NaCl, 1 mM $MgCl_2$, 0.5% NP40, 10 mM NaF, 0.2 mM $NaVO_4$, 10 mM β-glycerol phosphate, and 5%
403 glycerol) with freshly added dithiothreitol (DTT) (1 mM), PMSF (100 μM), and a protease inhibitor cocktail
404 (Roche, Branford, CT). The cells were incubated on ice for 30 minutes and sonicated using the Bioruptor
405 Ultra-sonication system (Diagenode, Denville, NJ). SDS-PAGE sample buffer was added to the sonicated
406 extracts and boiled. The samples were resolved by SDS-PAGE and transferred to PVDF membranes
407 (Millipore, Billerica, MA). The membranes were blotted with antibodies and then visualized using the
408 Immobilon Western Chemiluminescent reagent (Millipore) with the Bio-Rad ChemiDoc MP system (Bio-
409 Rad, Hercules, CA). The antibodies used in this study include PRMT1 (Cat# 07404, Millipore), LDHA (Cat#
410 MA5-17246, Invitrogen), p-LDHA (Cat# 8176, Cell Signaling), and CPT1a (Cat# 66039, Proteintech).

411 Quantitative Real-time PCR

412 Total RNA was prepared using Direct-Zol RNAprep Kit (Zymo research, Irvine, CA). cDNA was generated
413 by the Verso cDNA synthesis Kit (Thermo Scientific, Walthum, MA) with random hexamer priming. Real-
414 time PCR assays were performed with Absolute Blue qPCR SYBR Green Mix (Thermo Scientific) on a ViiA
415 7 system (Applied Biosystems, Waltham, MA). The relative quantity of gene expression was calculated by
416 the ΔΔCt method. Housekeeping gene ACTB (forward: GGC TGG CCG GGA CCT GAC AGA CTA C;
417 reverse: GCA GTG GCC ATC TCC TGC TCG AAG TC) was used for normalization.

418 Primer list:

Prmt1-F	CCCGTGGAGAAGGTGGACAT
Prmt1-R	CTCCCACCAGTGGATCTTGT
Cpt1a-F	GGCATAAACGCAGAGCATTCCTG
Cpt1a-R	CAGTGTCCATCCTCTGAGTAGC
Idha-F	GAATTACGATGGGGATGTGC

Idha-R GACGTCTCTTGCCCTTTCTG

Fasn-F AAGTTCGACGCCTCCTTTTT

Fasn-R TGCCTCTGAACCACTCACAC

419 Murine cytochrome B forward: CTTCATGTCGGACGAGGCTTA

420 Murine cytochrome B reverse: TGTGGCTATGACTGCGAACA

421 Cell Viability Assays

422 Cell viability was measured using the CellTiter-Glo Viability Assay Kit (Promega, Madison, WI). A total of
423 1,000 6133 cells were seeded in 96-well plates (100 μL per well) with or without treatment. At the specified
424 time after culture setup, 100 μL of CellTiter-Glo reagent was added to each well. The luminescent signal
425 was recorded with a microplate reader (Biotek, Winooski, VT).

426 Metabolite extraction

427 Cells were washed twice with ice-cold PBS before extracting metabolites in a 20% methanol
428 solution (LC-MS grade methanol, Fisher Scientific) at −70 °C. The tissue–methanol mixture
429 underwent bead-beating for 45 seconds using a Tissue/cell disruptor (Qiagen). The extracts were
430 centrifuged for 5 minutes at 2000Xg to pellet insoluble material, and the supernatants were
431 transferred to clean tubes. This extraction procedure was repeated two more times, and all three
432 supernatants were pooled, dried using a Vacufuge (Eppendorf), and stored at −80 °C until
433 analysis. The methanol-insoluble protein pellet was solubilized in 0.2 M NaOH at 95 °C for 20
434 minutes, and the total protein concentration was quantified using a BioRad DC assay. On the day
435 of metabolite analysis, the dried cell extracts were reconstituted in 70% acetonitrile to achieve a
436 relative protein concentration of 1 μg/ml, and 4 μl of this reconstituted extract was injected for
437 LC/MS-based untargeted metabolite profiling.

438 LC/MS metabolomics

439 Cell extracts were analyzed using an LC/MS system that featured an Agilent Model 1290 Infinity II
440 liquid chromatography platform coupled with an Agilent 6550 iFunnel time-of-flight mass
441 spectrometer. The chromatography of metabolites utilized aqueous normal phase (ANP)
442 chromatography on a Diamond Hydride column (Microsolv). The mobile phases consisted of: (A)
443 50% isopropanol with 0.025% acetic acid, and (B) 90% acetonitrile containing 5 mM ammonium
444 acetate. To minimize the interference of metal ions on chromatographic peak integrity

445 and electrospray ionization, EDTA was introduced to the mobile phase at a final concentration of
446 6 μM. The mobile phase gradient was as follows: 0–1.0 min, 99% B; 1.0–15.0 min, decreasing to
447 20% B; 15.0 to 29.0 min, 0% B; and from 29.1 to 37 min, returning to 99% B. Raw data were
448 analyzed with MassHunter Profinder 8.0 and MassProfiler Professional (MPP) 15.1 software
449 (Agilent Technologies).

450 Metabolite structure specification

451 To determine the identities of differentially expressed metabolites ($P < 0.05$), LC/MS data were queried
452 against an in-house annotated personal metabolite database, created using MassHunter PCDL Manager
453 8.0 (Agilent Technologies), based on monoisotopic neutral mass (<5 ppm mass accuracy) and
454 chromatographic retention times of pure standards. A molecular formula generator (MFG) algorithm in MPP
455 was utilized to generate and score empirical molecular formulas, considering monoisotopic mass accuracy,
456 isotope abundance ratios, and spacing between isotope peaks. A tentative compound ID was assigned
457 when the PCDL database and MFG scores matched for a given candidate molecule. Tentatively assigned
458 molecules were confirmed based on matching LC retention times and/or MS/MS fragmentation spectra for
459 pure molecular standards.

460 Seahorse Assays

461 The metabolic activities of living 6133 cells and 6133/PRMT1 cells were measured using a Seahorse XF24
462 metabolic flux analyzer (Agilent Technologies, Santa Clara, CA), following the described procedures(Yu et
463 al., 2013). Briefly, AMKL cells ($1.5\text{-}2 \times 10^5$) were seeded in 24-well plates designed for XF24 cell culture.
464 The plates were pre-coated with Cell-Tak (Corning, Corning, NY) and incubated in XF base medium
465 containing glucose (10 mM), L-glutamine (2 mM), and sodium pyruvate (1 mM) at 37°C for 1 hour. Oxygen
466 consumption rates (OCRs) were measured at baseline and after the sequential addition of the
467 mitochondrial inhibitor oligomycin (500 nM), the mitochondrial uncoupling compound FCCP (5 μM), and the
468 respiratory chain inhibitor antimycin (1 μM) to the culture. The FCCP concentration must be determined by
469 titration. Glycolytic activities were simultaneously assessed using the same instrument based on
470 extracellular acidification rates (ECARs). All measurements were conducted according to the
471 manufacturer's protocols, and the data were normalized by cell numbers.
472

473 Statistics and Data Analysis:
474 The figure legends provide all the experimental details. In the bar graphs, a 2-tailed Student's t-test was
475 employed for significance testing, with P values less than 0.05 deemed significant. Quantitative data are

476 presented as mean ± SEM. The R programming package and GraphPad Prism 6 were utilized for
477 statistical analysis.

478 **Figure 1. PRMT1 Promotes Leukemia Cell Transformation.**
479 A. 6133 cells were stained with E84, then FACS was sorted based on E84 intensity. $3x10^5$ sorted cells
480 were intravenously transferred to sublethally irradiated mice.
481 B. Leukemia progression in recipient mice was shown on Kaplan-Meier curves.
482 C. The manifestation of leukemia cells in the bone marrow and peripheral blood of recipient mice was
483 measured using flow cytometry. In the E84-low group, the bottom five dots represent five recipient mice
484 that were sacrificed on day 90 post-transfer. Closed symbols indicate moribund mice, while open symbols
485 denote non-terminally ill, inhibitor-treated mice sacrificed on day 88.
486 D. PRMT1 expression renders 6133 cells' cytokine-independent growth. 6133 cells and 6133/PRMT1 cells
487 were cultured with or without mouse stem cell factor (SCF). Cell viabilities were measured daily.
488 E. Schematic for inducing leukemia through the intravenous injection of 6133 or 6133/PRMT1 cells into
489 sub-lethally irradiated recipient mice (n=7).
490 F. Leukemia progression in recipient mice was documented on Kaplan-Meier curves.
491
492 **Figure 2. PRMT1 Inhibitor MS023 Blocks Leukemia Progression.**
493 A. The survival of 6133/PRMT1 cells is highly sensitive to treatment with MS023. Both 6133 and
494 6133/PRMT1 cells were treated with MS023 for 48 hours, and cell viability was determined by counting.
495 B. 6133/PRMT1 cells were intravenously transferred into sub-lethally irradiated mice. Recipient mice
496 received intraperitoneal injections of either a PRMT1 inhibitor or vehicle for 15 doses, given every other
497 day.
498 C. The progression of leukemia was illustrated on Kaplan-Meier curves. n=5.
499 D. Leukemia cells in recipient mice (n=6) were quantified using flow cytometry. The right panel shows the
500 weights of the spleens from recipient mice. Closed symbols represent moribund mice, and open symbols
501 represent non-terminally ill, inhibitor-treated mice that were sacrificed on days 40 and 120.
502 E. Peripheral blood was collected from non-terminally ill, inhibitor-treated mice at 40 and 120 days post-cell
503 transfer.
504 F. MS203 treatment of in vitro cultured 6133 and 6133/cMPLW515L cells. n=3. $P< 0.05$.
505 G. Schematic of leukemia induced by 6133 c-mplW515L transplantation.
506 H. Kaplan-Meier curves for MS023 treated leukemia mice induced by 6133 c-mplW515L cells. n=7.
507 I. The percentage of GFP-positive leukemia cells in the peripheral blood and bone marrow of the vector
508 and inhibitor-treated mice at the endpoints. ****$P<0.0001$.
509
510 **Figure 3. PRMT1 Promotes Glycolysis.**

511 A. Extracellular acidification rates (ECAR) in 6133 and 6133/PRMT1 cells were measured using Seahorse
512 assays. 150,000 cells were seeded in special 24-well plates for the Seahorse Xf-24 analyzer. Oligomycin,
513 FCCP, and antimycin were injected sequentially into the wells as indicated.
514 B. Extracellular acidification rates in PRMT1 inhibitor (MS023)- treated 6133 cells. Cells were pretreated
515 with MS023 overnight before Seahorse analysis.
516 C. The protein levels of lactate dehydrogenase A (LDHA) and p-Y10-LDHA in both 6133 and 6133/PRMT1
517 cells were assessed using Western blotting. The cells were cultured at the same density, and extracts were
518 harvested after an overnight incubation.
519 D. Intracellular and extracellular lactate levels were measured using an L-lactate kit. Cells were seeded at
520 $1x10^7$ cells/ml and cultured for 24 hours, followed by centrifugation. Both the medium/supernatant
521 (extracellular) and the cell pellet (intracellular) were collected for analysis. The results from the triplicates
522 are plotted. * $p < 0.05$.
523
524 **Figure 4. PRMT1 Changes Oxygen Consumption and Redox Status.**
525 A. Oxygen consumption rates (OCR) in 6133 and 6133/PRMT1 cells were measured using Seahorse assays.
526 A total of 150,000 cells were seeded in specialized 24-well plates designed for the Seahorse Xf-24 analyzer.
527 Oligomycin, FCCP, and antimycin were injected into the wells sequentially as indicated.
528 B. Oxygen consumption rates in PRMT1 inhibitor-treated 6133/PRMT1 cells. Cells were pretreated with
529 PRMT1 inhibitor MS023 overnight prior to Seahorse analysis.
530 C. Mitotracker Deep Red FM staining assessed the mitochondrial mass in 6133 and 6133/PRMT1 cells.
531 D. Quantitative PCR of mitochondria-specific gene cytochrome B measured the mitochondrial DNA amount.
532 E. TMRE staining was performed to measure mitochondrial membrane potential. Cells were seeded at
533 $1.1x10^5$ cells/ml, and 0.1 volume of 5mM TMRE was added to the culture to reach a final concentration of
534 500nM. After 20 minutes, cells were collected and used for FACS analysis.
535 F. The intracellular ROS level was measured by H2-DCFDA staining. $1x10^5$ cells were incubated in a warm
536 staining solution containing 10 uM of H2DCFDA for 30 minutes, then washed and subjected to analysis.
537 G. Mitochondrial ROS was measured by MitoSOX staining. 5x105 cells were incubated with a warm staining
538 solution containing 2.5 uM of MitoSOX for 10 minutes and then washed and subjected to analysis.
539 H. Intracellular levels of GSH/GSSG and NADP/NADPH ratio were measured. In each assay, $5x10^5$ cells
540 were used for extract preparation.
541
542 **Figure 5: Metabolomic analysis of PRMT1-regulated metabolism in 6133 cells.** 6133 cells expressing
543 doxycycline-inducible PRMT1 were induced to express PRMT1. The activated group (labelled as A):

544 metabolites collected after PRMT1 was induced. Control group (labelled as C): metabolites collected
545 before PRMT1 was induced.
546 A. principle component analysis (PCA) for the metabolites. The C group and A group were clustered at
547 different positions in PCA analysis.
548 B. heatmap of metabolites differentially expressed in these two groups.
549 C. volcano plots for metabolites. 204 metabolites are changed more than 2 folds with P <0.5.
550 D. Metabolic pathways are primarily influenced by PRMT1 overexpression in 6133 cells. The metabolite
551 data were analyzed using a web-based program called MetaboAnalystR6.0.

552 **Figure 6. PRMT1 Causes Leukemia Cells' Heavy Dependency on Glucose consumption.**
553 A. Colorimetric assay of glucose in 6133 and 6133/PRMT1 cells. 1.25x 105 cells were seeded per well and
554 cultured overnight. After centrifugation, the supernatant/medium was collected and used for the assay.
555 B. Cell viability of 6133 and 6133/PRMT1 cells under glucose-free conditions. Cells were seeded in a 96-
556 well plate with fresh regular or glucose-minus RPMI1640 medium. Cell viability was measured by CellTiter-
557 Glo kit. Ratios were normalized to the wells with regular RPMI-1640 medium.
558 C. Cell viability of 6133 and 6133/PRMT1 cells following 2-DG treatment. Cells were plated in 96-well
559 plates containing 2-DG. Cell viability was measured by CellTiter-Glo kit. The growth of cells without the
560 addition of 2-DG served as a normalization reference.
561 D. 6133/PRMT1 cells were transferred intravenously into sub-lethally irradiated mice. Beginning on day 4
562 post-transfer, recipient mice received intraperitoneal injections of saline or 0.25 g/kg body weight of 2-DG
563 every other day. The survival of recipient mice is presented as Kaplan-Meier curves.
564 E. The percentages of leukemia cells in the bone marrow and peripheral blood of recipient mice were
565 measured using flow cytometry. Closed symbols represent mice transplanted with 6133/PRMT1 cell-
566 induced leukemia, while the open square indicates a control wild-type mouse without leukemia.
567

568 **Figure 7. PRMT1 Alters Fatty Acid Oxidation in Leukemia Cells.**
569 A. The mRNA levels of CPT1a and PPARα in 6133 and 6133/PRMT1 cells were assessed. Cell pellets
570 were harvested in Trizol prior to RNA extraction, followed by cDNA synthesis and qPCR analysis.
571 B. Western blotting of 6133 and 6133/PRMT1 cell lines.
572 C. BODIPY/lipid Staining of 6133 Cells. Cells were incubated with 200 nM of BODIPY/lipid at 37°C for 15
573 minutes, then washed with medium and prepared for FACS analysis.
574 D. Cell viability of 6133 and 6133/PRMT1 cells with Etomoxir treatment. 6133 and 6133-PRMT1 cells were seeded in
575 a 96-well plate, supplemented with Etomoxir. Cell viability was measured by CellTiter-Glo Kit. Ratios were normalized
576 to day 0.
577 E. Cell viability of 6133 and 6133-PRMT1 cells with Orlistat treatment.
578 F. Viability of 6133 and 6133-PRMT1 cells with a supplement of short-chain fatty acid (triacetin/ tripropoinin/tributyrin)
579 under glucose-free conditions. Cells were cultured with RPMI with or without glucose, supplemented with 100nM of
580 triacetin/tripropionin/tributyrin, respectively. Cell viability was measured after 72 hours. Fold change of viability is
581 normalized to glucose+ cells.
582 G. Growth curves of 6133-PRMT1 cells transduced with CPT1A, CPT1A/H473A and CPT1A/G710E.
583

584 Supplemental Figure 1. Expression of metabolic regulated genes in cells with differential PRMT1
585 Expression levels.
586 A. Two populations of 6133 cells were FACS-sorted based on E84 staining intensity, as in Figure 1. Sorted
587 cells were harvested and subjected to western blotting.

588 B. RNA was extracted from sorted cells and used for quantitative real-time PCR.

589 Supplemental Figure 2. RBM15-MKL1 (OTT-MAL) Protein Stability is not Affected by PRMT1 Activity.
590 A. HEK293T cells were transfected with constructs expressing HA-tagged RBM15-MKL1 with or without
591 PRMT1. Extracts were harvested 24 hours post-transfection and then used for western blotting.
592 Endogenous RBM15 is indicated.
593 B. NB4 cells were treated with PRMT1 inhibitor MS023 for 24 hours. Extracts were harvested for western
594 blotting.
595 C. Global arginine di-methylation (Di-me-R) of bone marrow cells from mice injected with PRMT1 inhibitor
596 MS023. Mice were injected with 80 mg/kg body weight of MS023 or vehicle every other day for 30 days.
597 Bone marrow cells were collected, and extracts were prepared for western blotting.
598
599 Supplemental Figure 3. Responsiveness to Glucose Restriction of Cells with Differential PRMT1
600 Expression levels. FACS-sorted E84-high and E84-low 6133 cells were washed with fresh medium and
601 then seeded in glucose-free RPMI1640 medium for continuing culture. The viability of E84-high/low cells
602 was measured by CellTiter-Glo assay.

603

604

605 References:

606 Athale, U.H., Razzouk, B.I., Raimondi, S.C., Tong, X., Behm, F.G., Head, D.R., Srivastava, D.K., Rubnitz, J.E.,
607 Bowman, L., Pui, C.H., *et al.* (2001). Biology and outcome of childhood acute megakaryoblastic
608 leukemia: a single institution's experience. Blood *97*, 3727-3732.
609 Avasarala, S., Van Scoyk, M., Karuppusamy Rathinam, M.K., Zerayesus, S., Zhao, X., Zhang, W.,
610 Pergande, M.R., Borgia, J.A., DeGregori, J., Port, J.D., *et al.* (2015). PRMT1 is a Novel Regulator of
611 Epithelial-Mesenchymal-Transition in Non-Small Cell Lung Cancer. J Biol Chem.
612 Baldwin, R.M., Morettin, A., Paris, G., Goulet, I., and Cote, J. (2012). Alternatively spliced protein
613 arginine methyltransferase 1 isoform PRMT1v2 promotes the survival and invasiveness of breast
614 cancer cells. Cell Cycle *11*, 4597-4612.
615 Brejning, J., Jespersen, L., Arneborg, N., Brejning, J., Jespersen, L., and Arneborg, N. (2003-03-11).
616 Genome-wide transcriptional changes during the lag phase of Saccharomyces cerevisiae. Archives of
617 Microbiology 2003 179:4 *179*.
618 Butcher, R.A., Bhullar, B.S., Perlstein, E.O., Marsischky, G., LaBaer, J., and Schreiber, S.L. (2006).
619 Microarray-based method for monitoring yeast overexpression strains reveals small-molecule targets
620 in TOR pathway. Nat Chem Biol *2*, 103-109.
621 Chen, W.L., Wang, J.H., Zhao, A.H., Xu, X., Wang, Y.H., Chen, T.L., Li, J.M., Mi, J.Q., Zhu, Y.M., Liu, Y.F., *et al.*
622 (2014). A distinct glucose metabolism signature of acute myeloid leukemia with prognostic value.
623 Blood *124*, 1645-1654.
624 Chen, X., Sunkel, B., Wang, M., Kang, S., Wang, T., Gnanaprakasam, J.N.R., Liu, L., Cassel, T.A., Scott, D.A.,
625 Munoz-Cabello, A.M., *et al.* (2022). Succinate dehydrogenase/complex II is critical for metabolic and
626 epigenetic regulation of T cell proliferation and inflammation. Sci Immunol *7*, eabm8161.
627 Cheung, N., Chan, L.C., Thompson, A., Cleary, M.L., and So, C.W. (2007). Protein arginine-
628 methyltransferase-dependent oncogenesis. Nature cell biology *9*, 1208-1215.
629 Cho, E.C., Zheng, S., Munro, S., Liu, G., Carr, S.M., Moehlenbrink, J., Lu, Y.C., Stimson, L., Khan, O.,
630 Konietzny, R., *et al.* (2012a). Arginine methylation controls growth regulation by E2F-1. The EMBO
631 journal *31*, 1785-1797.
632 Cho, J.H., Lee, M.K., Yoon, K.W., Lee, J., Cho, S.G., and Choi, E.J. (2012b). Arginine methylation-
633 dependent regulation of ASK1 signaling by PRMT1. Cell Death Differ *19*, 859-870.
634 Cho, J.H., Lee, R., Kim, E., Choi, Y.E., and Choi, E.J. (2018). PRMT1 negatively regulates activation-
635 induced cell death in macrophages by arginine methylation of GAPDH. Exp Cell Res *368*, 50-58.
636 Choi, D., Oh, K.J., Han, H.S., Yoon, Y.S., Jung, C.Y., Kim, S.T., and Koo, S.H. (2012). Protein arginine
637 methyltransferase 1 regulates hepatic glucose production in a FoxO1-dependent manner. Hepatology
638 *56*, 1546-1556.
639 Divakaruni, A.S., Paradyse, A., Ferrick, D.A., Murphy, A.N., and Jastroch, M. (2014). Analysis and
640 interpretation of microplate-based oxygen consumption and pH data. Methods Enzymol *547*, 309-354.
641 Eram, M.S., Shen, Y., Szewczyk, M.M., Wu, H., Senisterra, G., Li, F., Butler, K.V., Kaniskan, H.U., Speed,
642 B.A., dela Sena, C., *et al.* (2016). A Potent, Selective, and Cell-Active Inhibitor of Human Type I Protein
643 Arginine Methyltransferases. ACS Chem Biol *11*, 772-781.
644 Fan, J., Hitosugi, T., Chung, T.W., Xie, J., Ge, Q., Gu, T.L., Polakiewicz, R.D., Chen, G.Z., Boggon, T.J., Lonial,
645 S., *et al.* (2011). Tyrosine phosphorylation of lactate dehydrogenase A is important for NADH/NAD(+)
646 redox homeostasis in cancer cells. Molecular and cellular biology *31*, 4938-4950.
647 Faubert, B., Solmonson, A., and DeBerardinis, R.J. (2020). Metabolic reprogramming and cancer
648 progression. Science *368*.

649 Ferrer, C.M., Lynch, T.P., Sodi, V.L., Falcone, J.N., Schwab, L.P., Peacock, D.L., Vocadlo, D.J., Seagroves,
650 T.N., and Reginato, M.J. (2014). O-GlcNAcylation regulates cancer metabolism and survival stress
651 signaling via regulation of the HIF-1 pathway. Mol Cell *54*, 820-831.
652 Fisk, J.C., and Read, L.K. (2011). Protein arginine methylation in parasitic protozoa. Eukaryotic cell *10*,
653 1013-1022.
654 Fong, J.Y., Pignata, L., Goy, P.A., Kawabata, K.C., Lee, S.C., Koh, C.M., Musiani, D., Massignani, E., Kotini,
655 A.G., Penson, A.*, et al.* (2019). Therapeutic Targeting of RNA Splicing Catalysis through Inhibition of
656 Protein Arginine Methylation. Cancer Cell *36*, 194-209 e199.
657 Guendel, I., Carpio, L., Pedati, C., Schwartz, A., Teal, C., Kashanchi, F., and Kehn-Hall, K. (2010).
658 Methylation of the tumor suppressor protein, BRCA1, influences its transcriptional cofactor function.
659 PloS one *5*, e11379.
660 Hayashi, Y., Zhang, Y., Yokota, A., Yan, X., Liu, J., Choi, K., Li, B., Sashida, G., Peng, Y., Xu, Z.*, et al.* (2018).
661 Pathobiological Pseudohypoxia as a Putative Mechanism Underlying Myelodysplastic Syndromes.
662 Cancer Discov *8*, 1438-1457.
663 He, X., Zhu, Y., Lin, Y.C., Li, M., Du, J., Dong, H., Sun, J., Zhu, L., Wang, H., Ding, Z.*, et al.* (2019). PRMT1-
664 mediated FLT3 arginine methylation promotes maintenance of FLT3-ITD(+) acute myeloid leukemia.
665 Blood *134*, 548-560.
666 Humpton, T.J., Hock, A.K., Maddocks, O.D.K., and Vousden, K.H. (2018). p53-mediated adaptation to
667 serine starvation is retained by a common tumour-derived mutant. Cancer Metab *6*, 18.
668 Jones, C.L., Stevens, B.M., D'Alessandro, A., Reisz, J.A., Culp-Hill, R., Nemkov, T., Pei, S., Khan, N., Adane,
669 B., Ye, H.*, et al.* (2019). Inhibition of Amino Acid Metabolism Selectively Targets Human Leukemia
670 Stem Cells. Cancer Cell *35*, 333-335.
671 Kafkova, L., Tu, C., Pazzo, K.L., Smith, K.P., Debler, E.W., Paul, K.S., Qu, J., and Read, L.K. (2018).
672 Trypanosoma brucei PRMT1 Is a Nucleic Acid Binding Protein with a Role in Energy Metabolism and
673 the Starvation Stress Response. MBio *9*.
674 Kalaitzidis, D., Sykes, S.M., Wang, Z., Punt, N., Tang, Y., Ragu, C., Sinha, A.U., Lane, S.W., Souza, A.L., Clish,
675 C.B.*, et al.* (2012). mTOR complex 1 plays critical roles in hematopoiesis and Pten-loss-evoked
676 leukemogenesis. Cell Stem Cell *11*, 429-439.
677 Karkhanis, V., Hu, Y.J., Baiocchi, R.A., Imbalzano, A.N., and Sif, S. (2011). Versatility of PRMT5-induced
678 methylation in growth control and development. Trends in biochemical sciences.
679 Kreitz, J., Schonfeld, C., Seibert, M., Stolp, V., Alshamleh, I., Oellerich, T., Steffen, B., Schwalbe, H.,
680 Schnutgen, F., Kurrle, N.*, et al.* (2019). Metabolic Plasticity of Acute Myeloid Leukemia. Cells *8*.
681 Kurmi, K., Hitosugi, S., Wiese, E.K., Boakye-Agyeman, F., Gonsalves, W.I., Lou, Z., Karnitz, L.M., Goetz,
682 M.P., and Hitosugi, T. (2018). Carnitine Palmitoyltransferase 1A Has a Lysine Succinyltransferase
683 Activity. Cell Rep *22*, 1365-1373.
684 L, M.G., Boulay, K., Topisirovic, I., Huot, M.E., and Mallette, F.A. (2017). Oncogenic Activities of IDH1/2
685 Mutations: From Epigenetics to Cellular Signaling. Trends Cell Biol *27*, 738-752.
686 Lagadinou, E.D., Sach, A., Callahan, K., Rossi, R.M., Neering, S.J., Minhajuddin, M., Ashton, J.M., Pei, S.,
687 Grose, V., O'Dwyer, K.M.*, et al.* (2013). BCL-2 inhibition targets oxidative phosphorylation and
688 selectively eradicates quiescent human leukemia stem cells. Cell Stem Cell *12*, 329-341.
689 Laplante, M., and Sabatini, D.M. (2013). Regulation of mTORC1 and its impact on gene expression at a
690 glance. Journal of cell science *126*, 1713-1719.
691 Le Romancer, M., Treilleux, I., Leconte, N., Robin-Lespinasse, Y., Sentis, S., Bouchekioua-Bouzaghou, K.,
692 Goddard, S., Gobert-Gosse, S., and Corbo, L. (2008). Regulation of estrogen rapid signaling through
693 arginine methylation by PRMT1. Mol Cell *31*, 212-221.

694 Lin, W.J., Gary, J.D., Yang, M.C., Clarke, S., and Herschman, H.R. (1996). The mammalian immediate-
695 early TIS21 protein and the leukemia-associated BTG1 protein interact with a protein-arginine N-
696 methyltransferase. J Biol Chem *271*, 15034-15044.
697 Liu, H., Chen, X., Wang, P., Chen, M., Deng, C., Qian, X., Bai, J., Li, Z., and Yu, X. (2024). PRMT1-mediated
698 PGK1 arginine methylation promotes colorectal cancer glycolysis and tumorigenesis. Cell Death Dis
699 *15*, 170.
700 Liu, L., Zhang, K., Sandoval, H., Yamamoto, S., Jaiswal, M., Sanz, E., Li, Z., Hui, J., Graham, B.H., Quintana,
701 A.*, et al.* (2015). Glial lipid droplets and ROS induced by mitochondrial defects promote
702 neurodegeneration. Cell *160*, 177-190.
703 Ma, Z., Morris, S.W., Valentine, V., Li, M., Herbrick, J.A., Cui, X., Bouman, D., Li, Y., Mehta, P.K., Nizetic, D.*,*
704 *et al.* (2001). Fusion of two novel genes, RBM15 and MKL1, in the t(1;22)(p13;q13) of acute
705 megakaryoblastic leukemia. Nat Genet *28*, 220-221.
706 Menendez, J.A., and Lupu, R. (2007). Fatty acid synthase and the lipogenic phenotype in cancer
707 pathogenesis. Nature reviews Cancer *7*, 763-777.
708 Mercher, T., Coniat, M.B., Monni, R., Mauchauffe, M., Nguyen Khac, F., Gressin, L., Mugneret, F., Leblanc,
709 T., Dastugue, N., Berger, R.*, et al.* (2001). Involvement of a human gene related to the Drosophila spen
710 gene in the recurrent t(1;22) translocation of acute megakaryocytic leukemia. Proc Natl Acad Sci U S A
711 *98*, 5776-5779.
712 Mercher, T., Raffel, G.D., Moore, S.A., Cornejo, M.G., Baudry-Bluteau, D., Cagnard, N., Jesneck, J.L.,
713 Pikman, Y., Cullen, D., Williams, I.R.*, et al.* (2009). The OTT-MAL fusion oncogene activates RBPJ-
714 mediated transcription and induces acute megakaryoblastic leukemia in a knockin mouse model. The
715 Journal of clinical investigation *119*, 852-864.
716 Messier, V., Zenklusen, D., and Michnick, S.W. (2013). A nutrient-responsive pathway that determines
717 M phase timing through control of B-cyclin mRNA stability. Cell *153*, 1080-1093.
718 Mitchell, T.R., Glenfield, K., Jeyanthan, K., and Zhu, X.D. (2009). Arginine methylation regulates
719 telomere length and stability. Mol Cell Biol *29*, 4918-4934.
720 Pang, Z., Lu, Y., Zhou, G., Hui, F., Xu, L., Viau, C., Spigelman, A.F., MacDonald, P.E., Wishart, D.S., Li, S.*, et*
721 *al.* (2024). MetaboAnalyst 6.0: towards a unified platform for metabolomics data processing, analysis
722 and interpretation. Nucleic Acids Res *52*, W398-W406.
723 Roberts, G.G., and Hudson, A.P. (2006). Transcriptome profiling of Saccharomyces cerevisiae during a
724 transition from fermentative to glycerol-based respiratory growth reveals extensive metabolic and
725 structural remodeling. Mol Genet Genomics *276*, 170-186.
726 Samudio, I., Harmancey, R., Fiegl, M., Kantarjian, H., Konopleva, M., Korchin, B., Kaluarachchi, K.,
727 Bornmann, W., Duvvuri, S., Taegtmeyer, H.*, et al.* (2010). Pharmacologic inhibition of fatty acid
728 oxidation sensitizes human leukemia cells to apoptosis induction. The Journal of clinical investigation
729 *120*, 142-156.
730 Schwartzenberg-Bar-Yoseph, F., Armoni, M., and Karnieli, E. (2004). The tumor suppressor p53 down-
731 regulates glucose transporters GLUT1 and GLUT4 gene expression. Cancer Res *64*, 2627-2633.
732 Sha, L., Daitoku, H., Araoi, S., Kaneko, Y., Takahashi, Y., Kako, K., and Fukamizu, A. (2016). Asymmetric
733 Arginine Dimethylation Modulates Mitochondrial Energy Metabolism and Homeostasis in
734 Caenorhabditis elegans. Molecular and cellular biology.
735 Shia, W.J., Okumura, A.J., Yan, M., Sarkeshik, A., Lo, M.C., Matsuura, S., Komeno, Y., Zhao, X., Nimer, S.D.,
736 Yates, J.R., 3rd*, et al.* (2012). PRMT1 interacts with AML1-ETO to promote its transcriptional
737 activation and progenitor cell proliferative potential. Blood *119*, 4953-4962.

738 Su, H., Jiang, M., Senevirathne, C., Aluri, S., Zhang, T., Guo, H., Xavier-Ferrucio, J., Jin, S., Tran, N.T., Liu,
739 S.M., *et al.* (2021). Methylation of dual-specificity phosphatase 4 controls cell differentiation. Cell Rep
740 *36*, 109421.
741 Su, H., Sun, C.W., Liu, S.M., He, X., Hu, H., Pawlik, K.M., Townes, T.M., Han, X., Klug, C.A., Henary, M., *et al.*
742 (2018). Defining the epigenetic status of blood cells using a cyanine-based fluorescent probe for
743 PRMT1. Blood Adv *2*, 2829-2836.
744 Thiollier, C., Lopez, C.K., Gerby, B., Ignacimouttou, C., Poglio, S., Duffourd, Y., Guegan, J., Rivera-Munoz,
745 P., Bluteau, O., Mabialah, V., *et al.* (2012). Characterization of novel genomic alterations and
746 therapeutic approaches using acute megakaryoblastic leukemia xenograft models. J Exp Med *209*,
747 2017-2031.
748 Wang, H., Huang, Z.Q., Xia, L., Feng, Q., Erdjument-Bromage, H., Strahl, B.D., Briggs, S.D., Allis, C.D.,
749 Wong, J., Tempst, P., *et al.* (2001). Methylation of histone H4 at arginine 3 facilitating transcriptional
750 activation by nuclear hormone receptor. Science *293*, 853-857.
751 Wang, K., Luo, L., Fu, S., Wang, M., Wang, Z., Dong, L., Wu, X., Dai, L., Peng, Y., Shen, G., *et al.* (2023).
752 PHGDH arginine methylation by PRMT1 promotes serine synthesis and represents a therapeutic
753 vulnerability in hepatocellular carcinoma. Nat Commun *14*, 1011.
754 Watanuki, S., Kobayashi, H., Sugiura, Y., Yamamoto, M., Karigane, D., Shiroshita, K., Sorimachi, Y., Fujita,
755 S., Morikawa, T., Koide, S., *et al.* (2024). Context-dependent modification of PFKFB3 in hematopoietic
756 stem cells promotes anaerobic glycolysis and ensures stress hematopoiesis. Elife *12*.
757 Yamamoto, T., Hayashida, T., Masugi, Y., Oshikawa, K., Hayakawa, N., Itoh, M., Nishime, C., Suzuki, M.,
758 Nagayama, A., Kawai, Y., *et al.* (2024). PRMT1 Sustains De Novo Fatty Acid Synthesis by Methylating
759 PHGDH to Drive Chemoresistance in Triple-Negative Breast Cancer. Cancer Res *84*, 1065-1083.
760 Yang, Y., and Bedford, M.T. (2013). Protein arginine methyltransferases and cancer. Nature reviews
761 Cancer *13*, 37-50.
762 Yoshimatsu, M., Toyokawa, G., Hayami, S., Unoki, M., Tsunoda, T., Field, H.I., Kelly, J.D., Neal, D.E.,
763 Maehara, Y., Ponder, B.A., *et al.* (2011). Dysregulation of PRMT1 and PRMT6, Type I arginine
764 methyltransferases, is involved in various types of human cancers. Int J Cancer *128*, 562-573.
765 Yu, W.M., Liu, X., Shen, J., Jovanovic, O., Pohl, E.E., Gerson, S.L., Finkel, T., Broxmeyer, H.E., and Qu, C.K.
766 (2013). Metabolic regulation by the mitochondrial phosphatase PTPMT1 is required for
767 hematopoietic stem cell differentiation. Cell Stem Cell *12*, 62-74.
768 Zhang, L., Tran, N.T., Su, H., Wang, R., Lu, Y., Tang, H., Aoyagi, S., Guo, A., Khodadadi-Jamayran, A., Zhou,
769 D., *et al.* (2015). Cross-talk between PRMT1-mediated methylation and ubiquitylation on RBM15
770 controls RNA splicing. Elife *4*, e07938.
771 Zhao, X., Jankovic, V., Gural, A., Huang, G., Pardanani, A., Menendez, S., Zhang, J., Dunne, R., Xiao, A.,
772 Erdjument-Bromage, H., *et al.* (2008). Methylation of RUNX1 by PRMT1 abrogates SIN3A binding and
773 potentiates its transcriptional activity. Genes Dev *22*, 640-653.
774 Zhu, Y., He, X., Lin, Y.C., Dong, H., Zhang, L., Chen, X., Wang, Z., Shen, Y., Li, M., Wang, H., *et al.* (2019).
775 Targeting PRMT1-mediated FLT3 methylation disrupts maintenance of MLL-rearranged acute
776 lymphoblastic leukemia. Blood *134*, 1257-1268.
777 Zou, L., Zhang, H., Du, C., Liu, X., Zhu, S., Zhang, W., Li, Z., Gao, C., Zhao, X., Mei, M., *et al.* (2012).
778 Correlation of SRSF1 and PRMT1 expression with clinical status of pediatric acute lymphoblastic
779 leukemia. Journal of hematology & oncology *5*, 42.

780

Graphic Abstract:

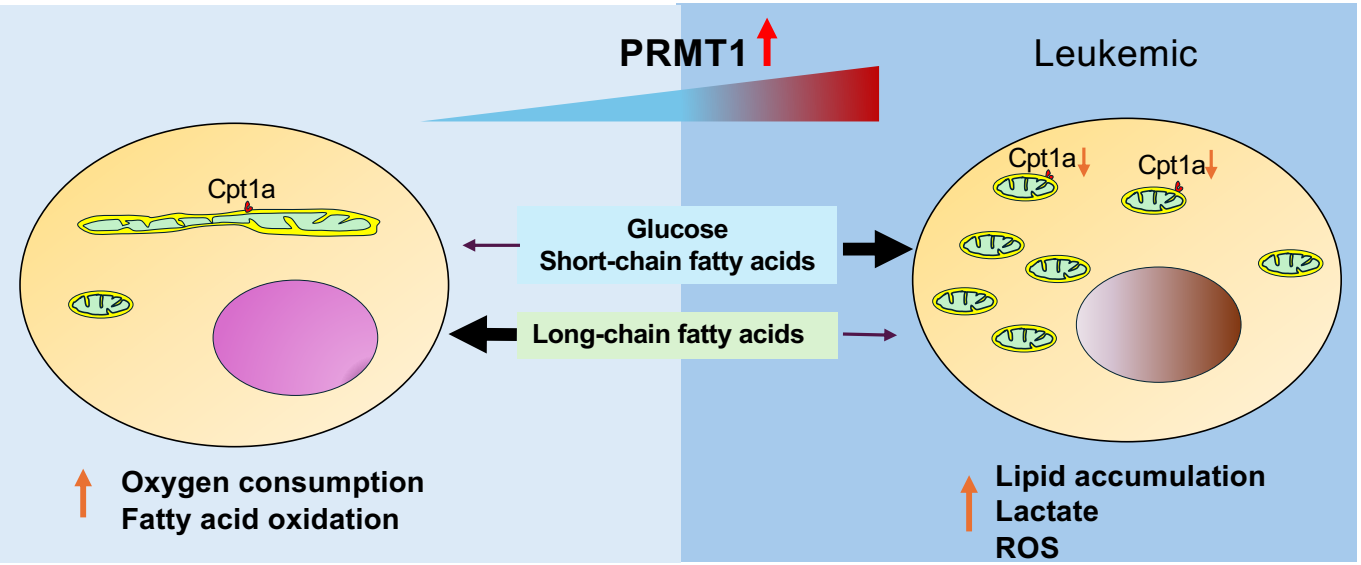

Su et a. Figure 1

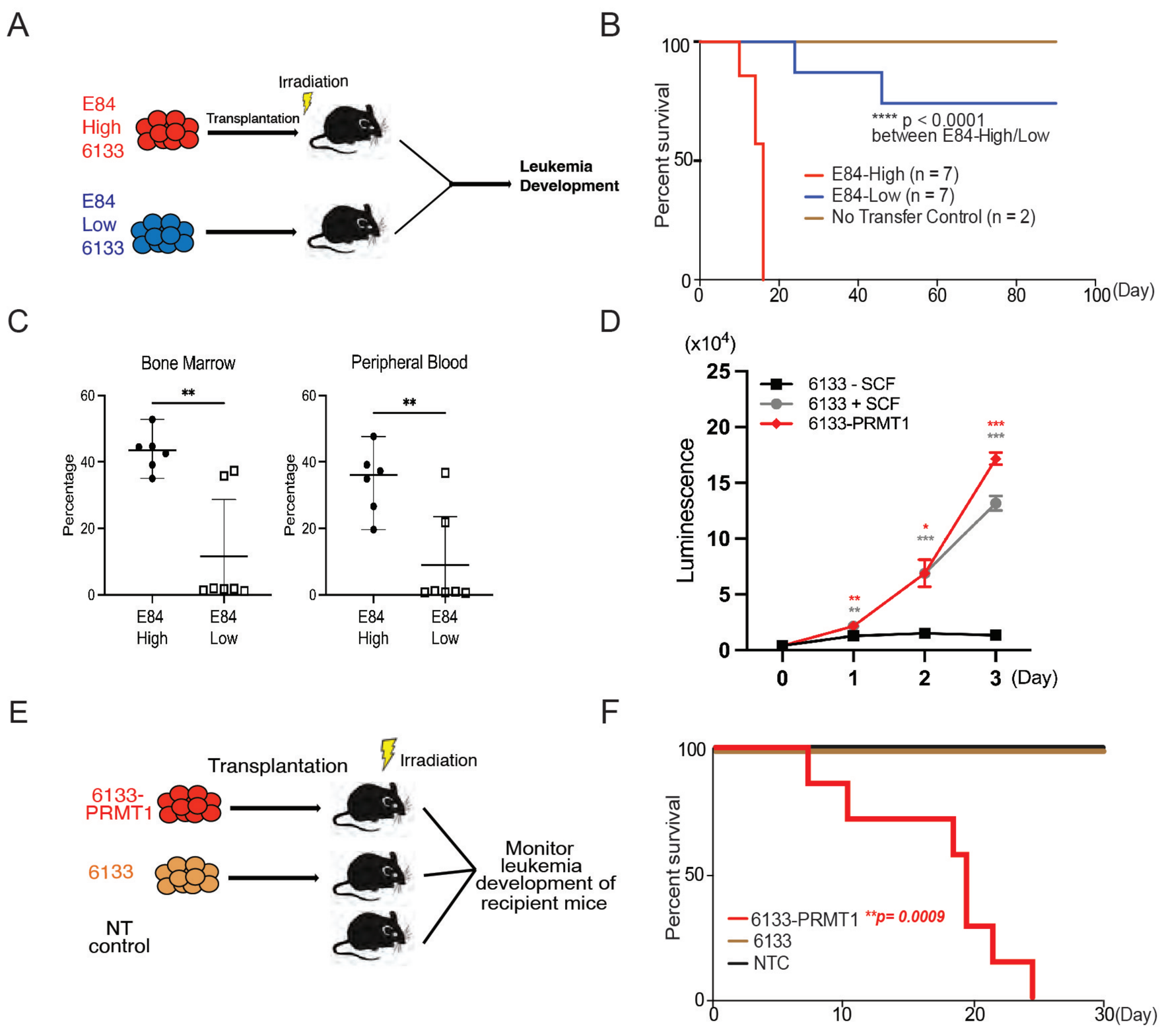

Su et al Figure 2

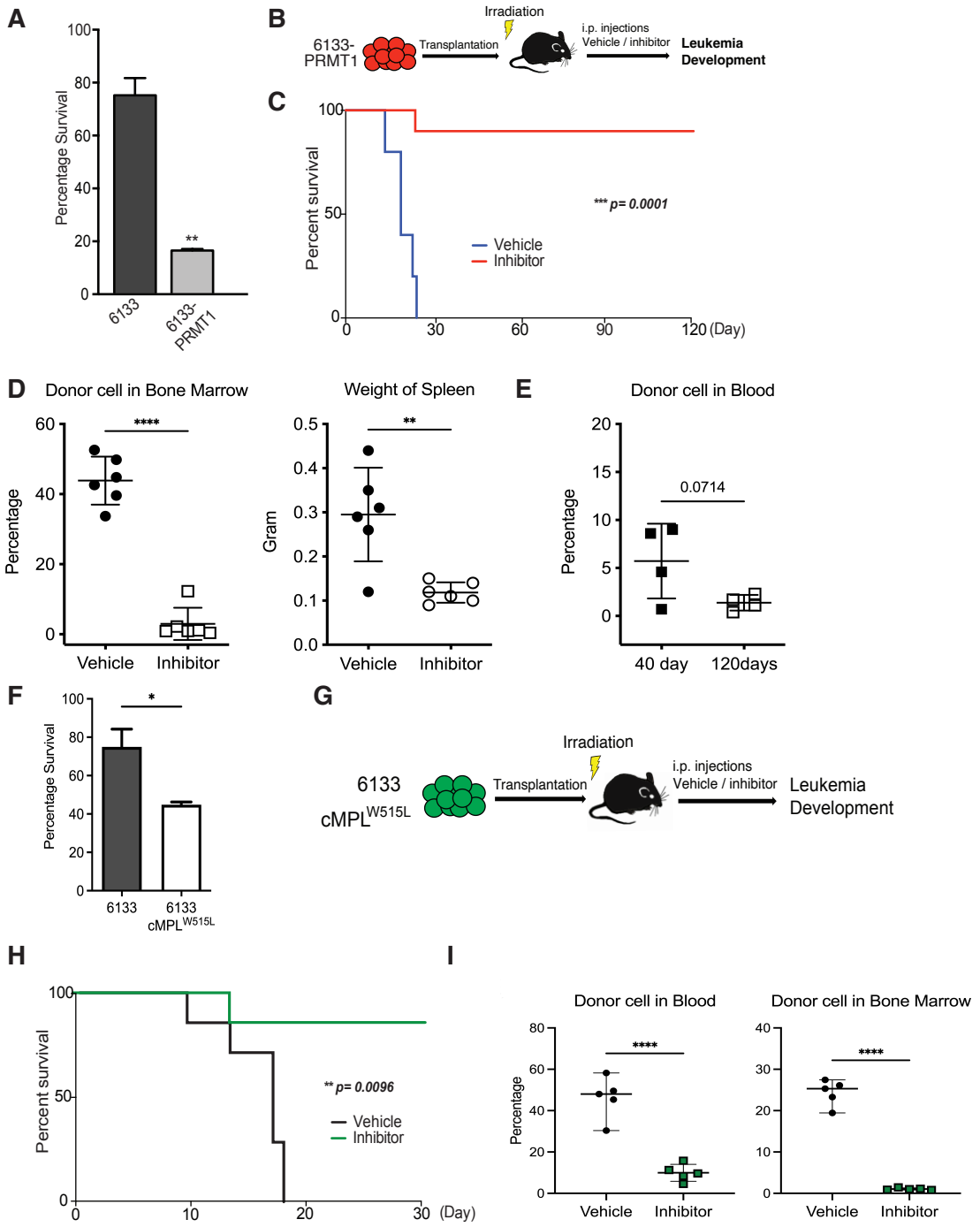

Su. et. al. Figure 3

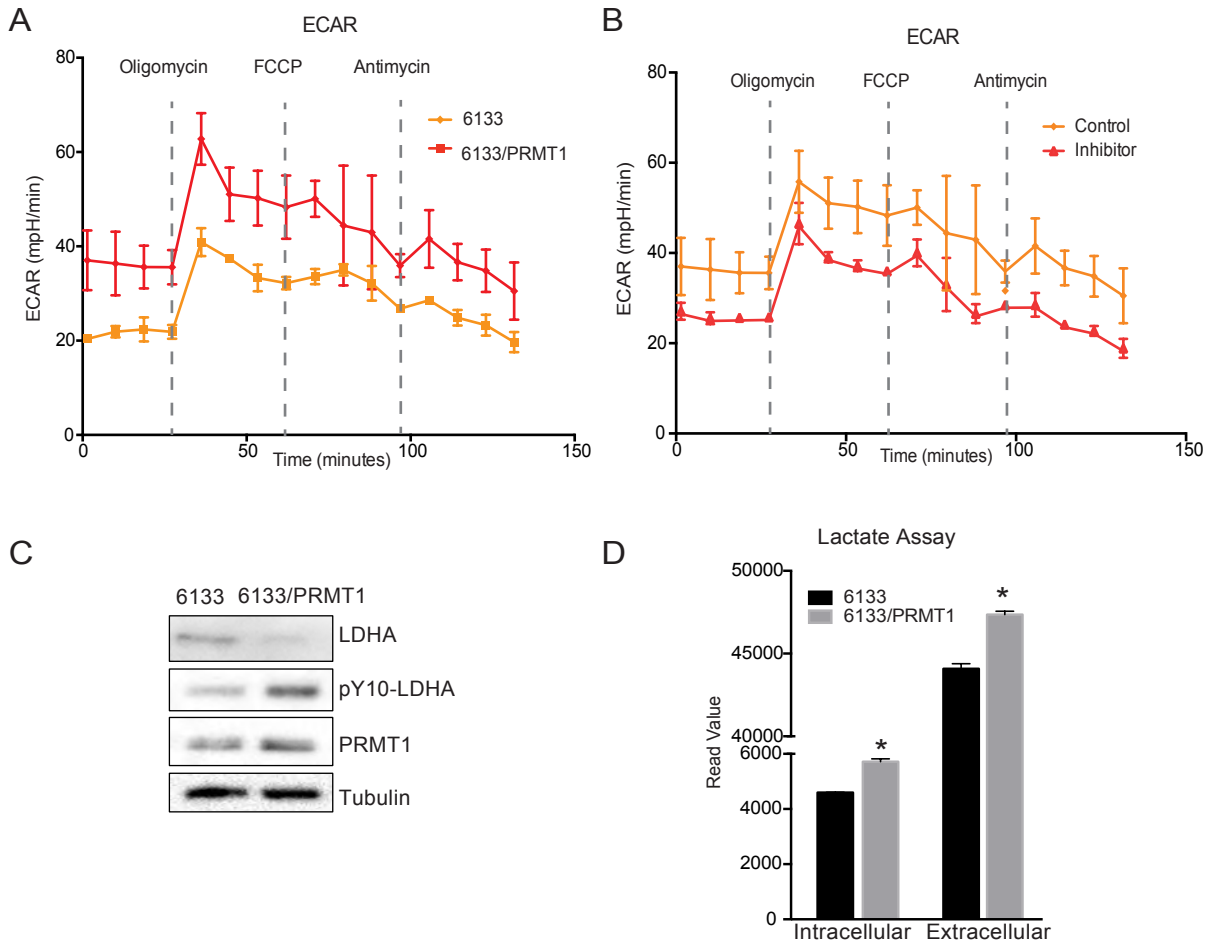

Su. et. al. Figure 4

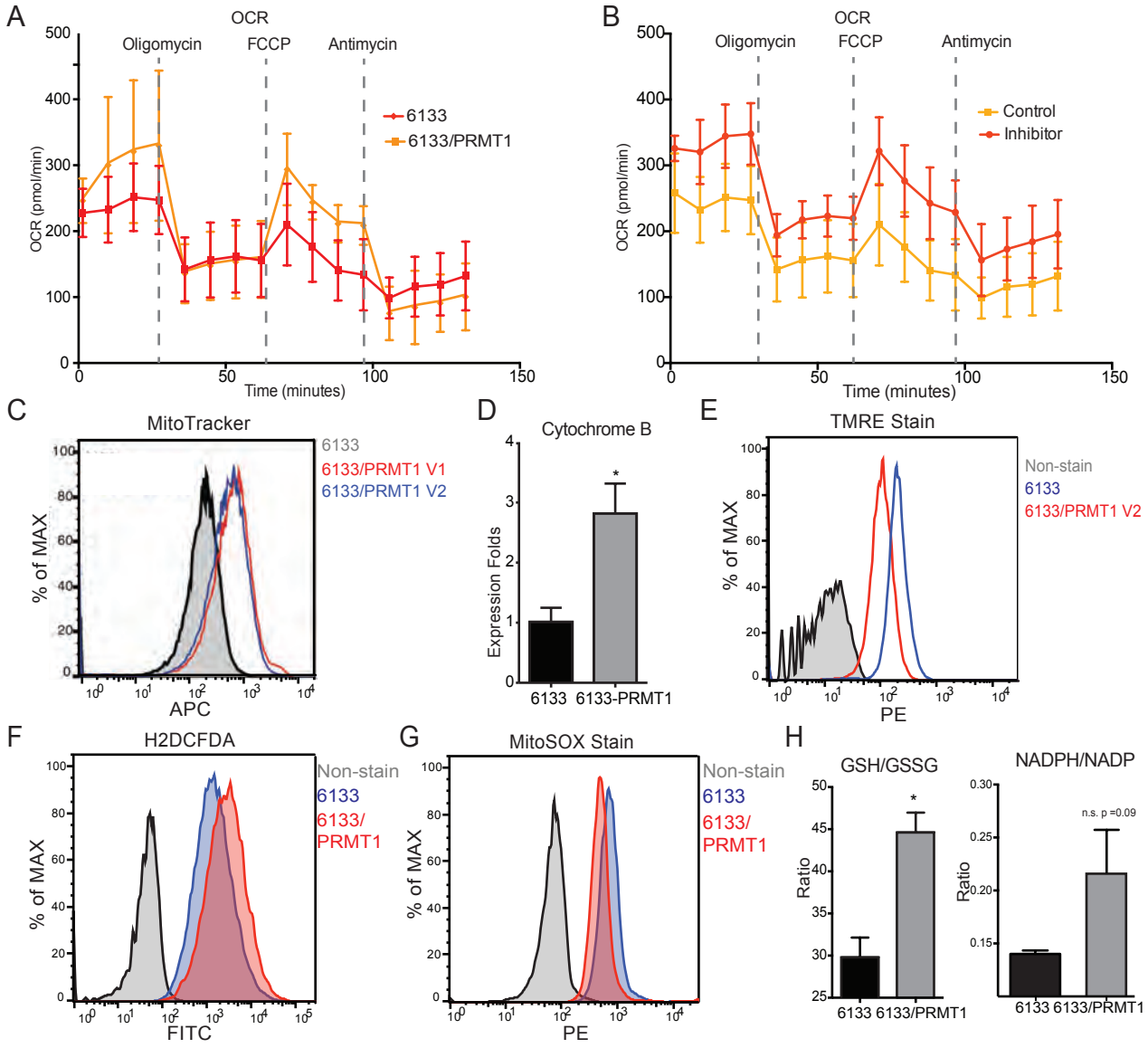

Figure 5.

A

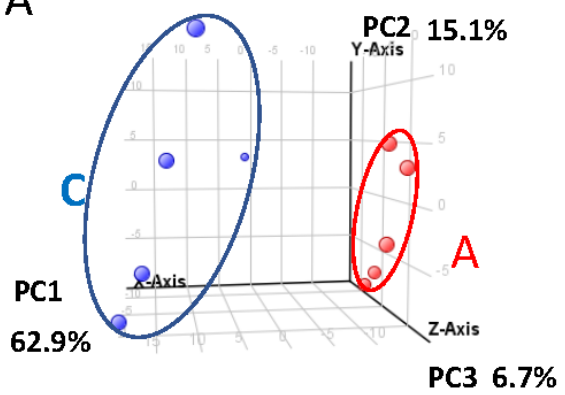

B

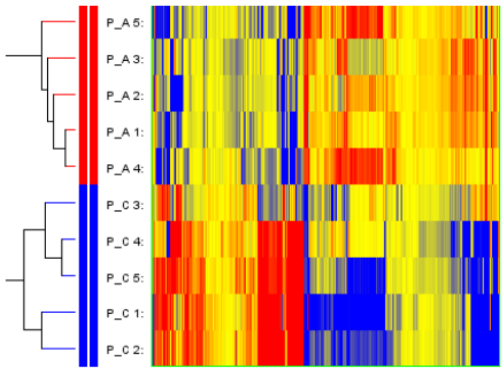

C

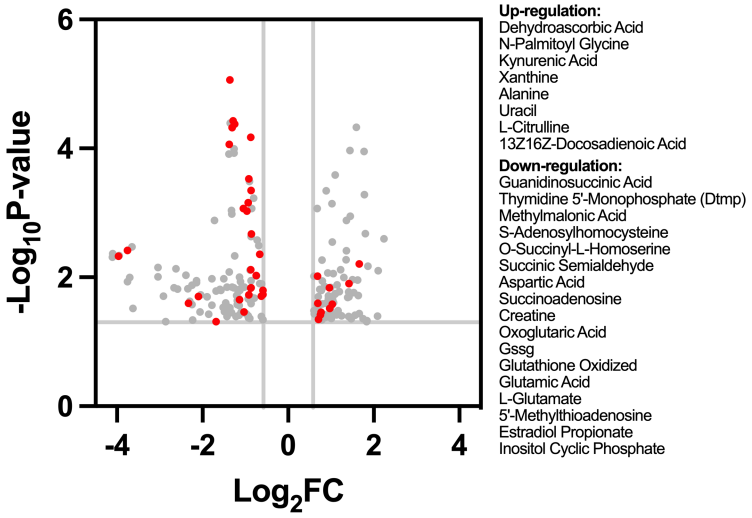

D

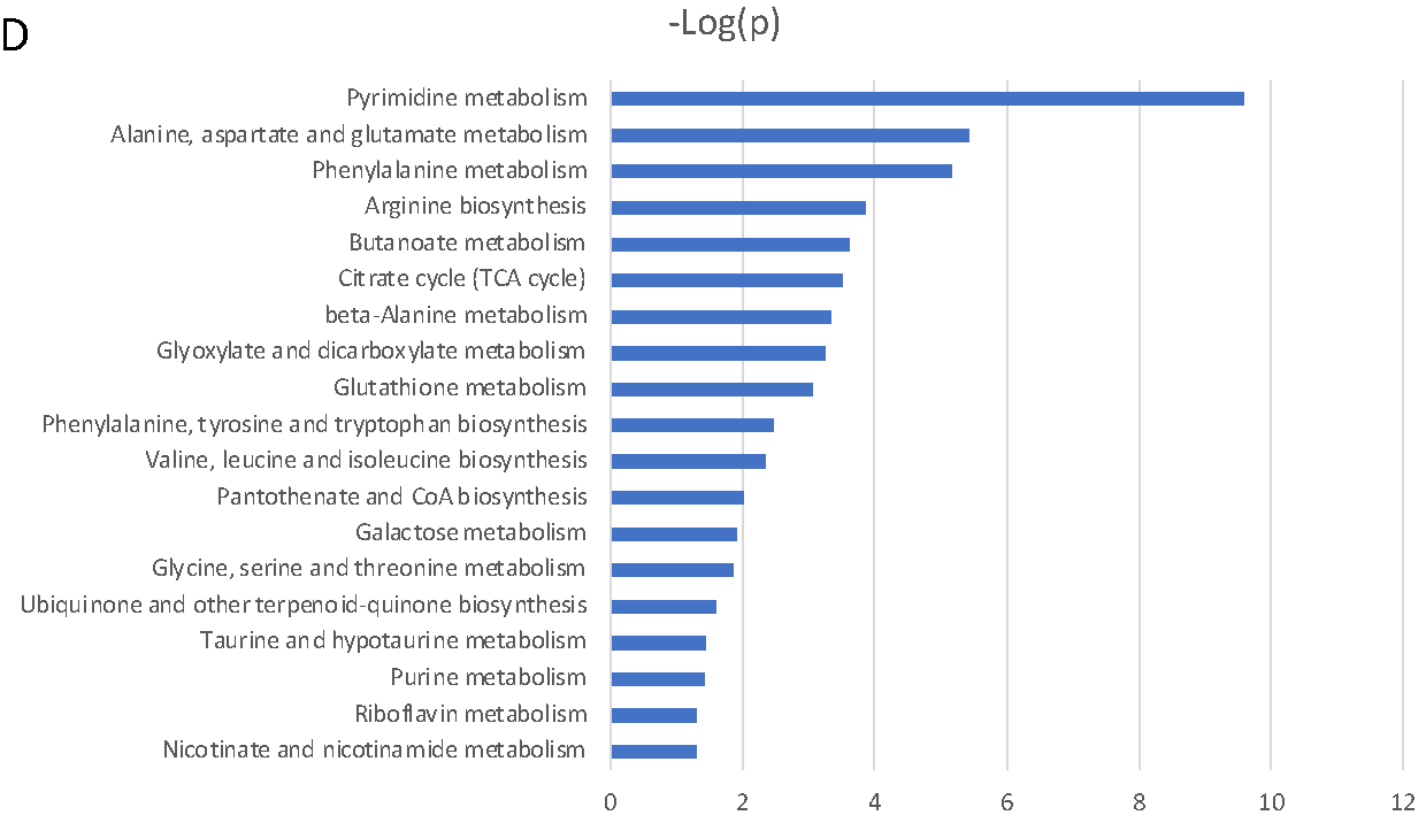

Su. et. al. Figure 6

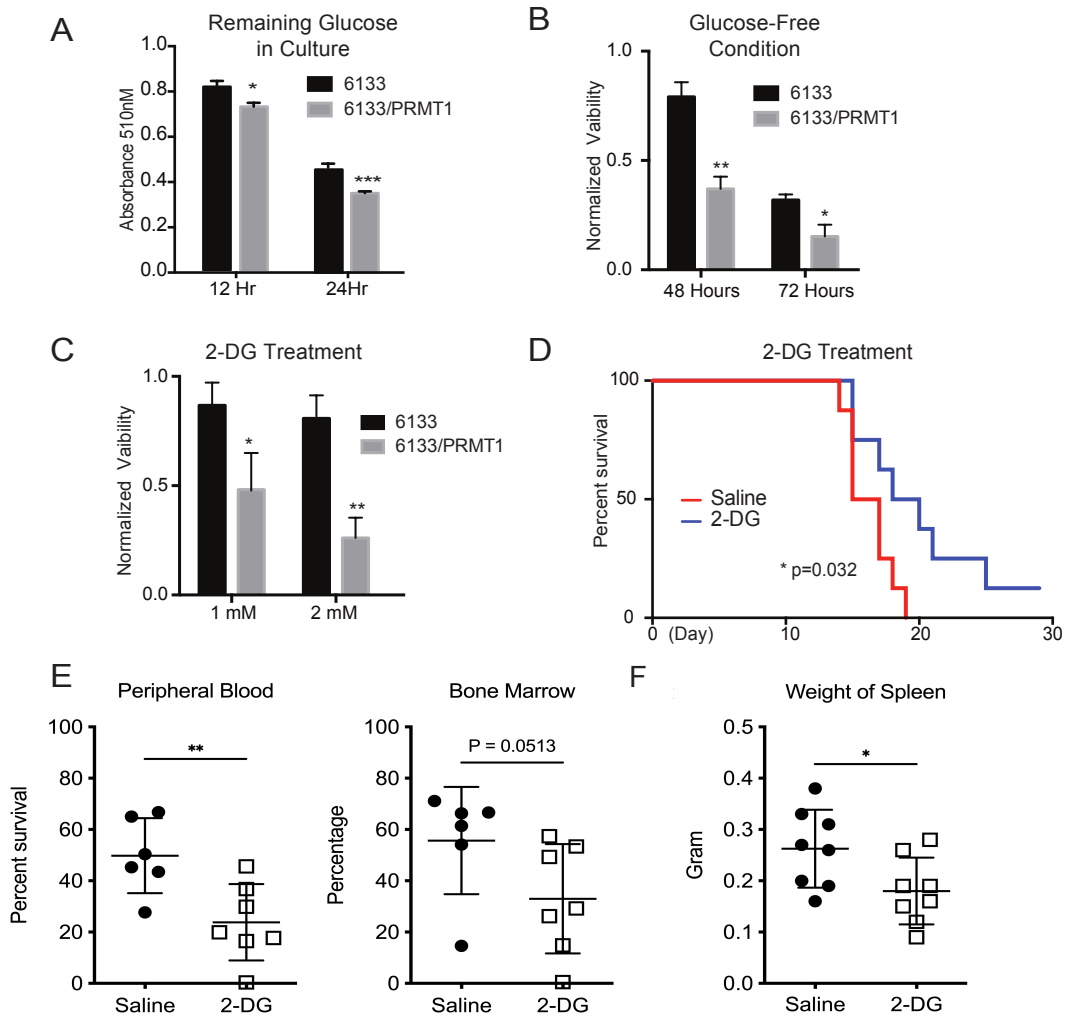

Su. et. al. Figure 7

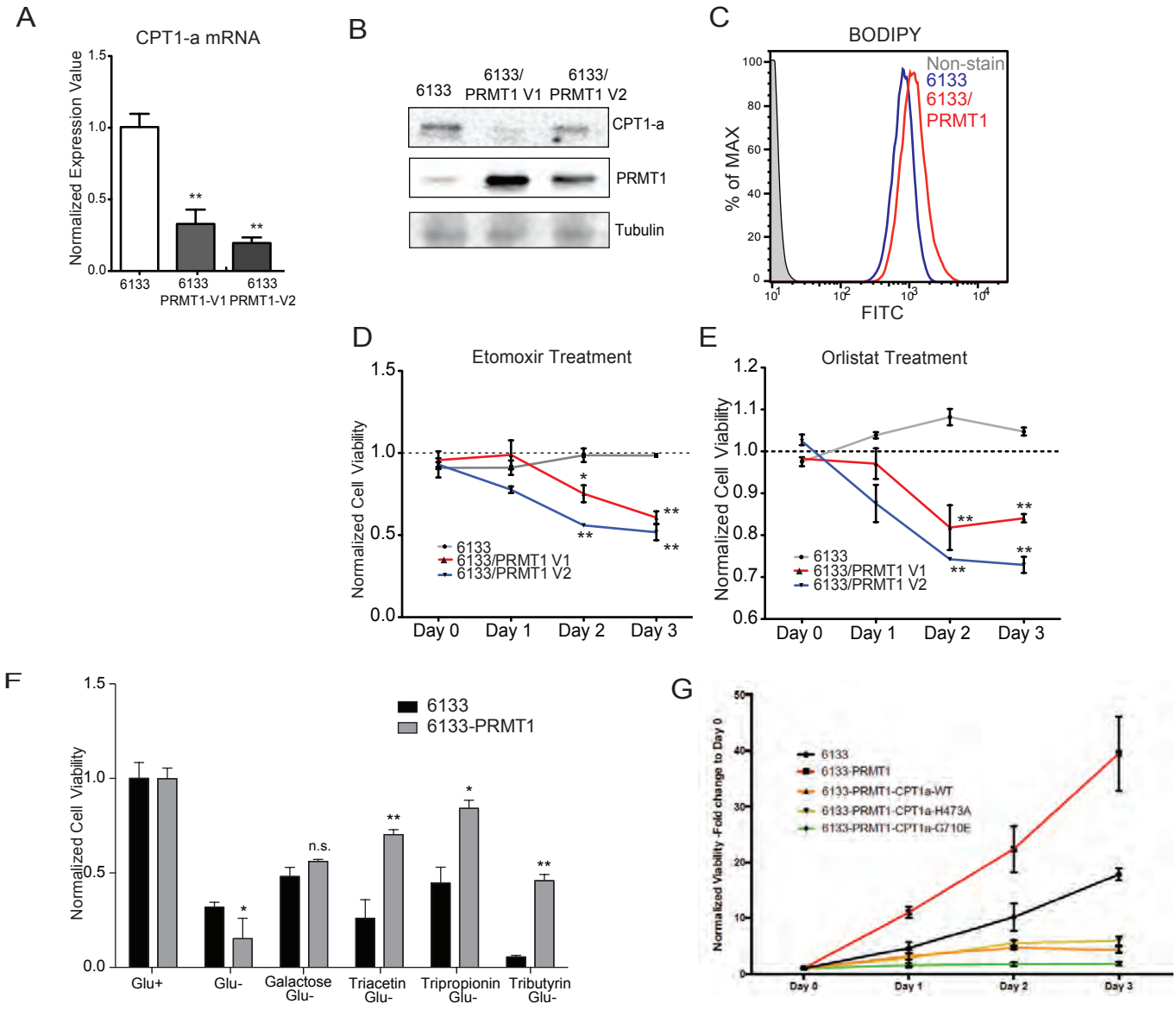

Su. et. al. Supplemental Figure 1

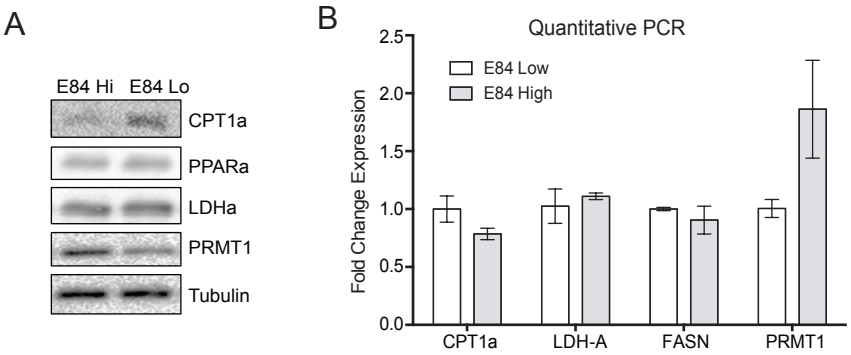

Supplemental Figure 2. Gene Expression of Cells with differential PRMT1 expression .
(A) 6133 was FACS sorted based on E84 staining intensity, as in Figure 1. Post-sort cells
were harvested and subjected to western blotting.
(B) RNA was extracted from sorted cells and used for quantitative-PCR.

Su. et. al. Supplemental Figure 2

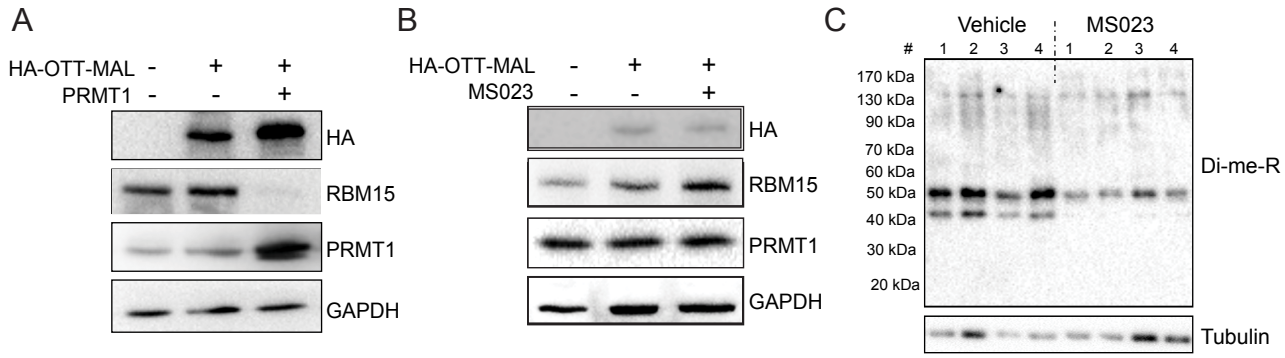

Supplemental Figure 2. RBM15-MKL1 (OTT-MAL) Protein Stability is not Affected by PRMT1 Activity.

A. HEK293T were transfected with constructs expressing HA-tagged RBM15-MKL1 with or without PRMT1. Extracts were harvested at 24 hours post transfection and then used for western blotting. Endogenous RBM15 is indicated.

(B) NB4 cells were treated with PRMT1 inhibitor MS023 for 24 hours. Extracts were harvested for western blotting.

C. Global arginine di-methylation (Di-me-R) of bone marrow cells from mice injected with PRMT1 inhibitor MS023. Mice were injected with 80 mg/kg body weight of MS023 or vehicle every other day, for 30 days. Bone marrow cells were collected and extracts were prepared for western blotting.

Su. et. al. Supplemental Figure 3

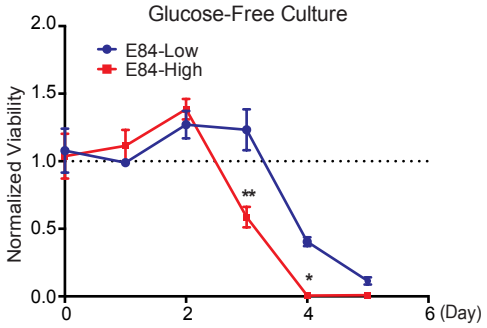

Supplemental Figure 3. Responsiveness to Glucose Restriction of Cells with Differential PRMT1 Expression .
FACS-sorted E84-high and E84-low 6133 cells were washed with fresh medium and then seeded in glucose-free RPMI1640 medium for continuing culture. Viability of E84-high/low cells were measured by CellTiter-Glo assay.